Physics of Materials

GaN

screw + mixed

Chapter 10: TEM techniques for characterizing dislocations

Dr. Thomas LaGrange

LUMES

Masters Course PHYS-307

Fall 2025

thomas.lagrange@epfl.ch • www.epfl.ch• lumes.epfl.ch• moodle.epfl.ch• PHYS-307

High energy electrons provide high spatial resolution

L. de Broglie (1924) postulates that p=h/ λ is valid for all particles λ wavelength of electrons (Nobel prize 1929)

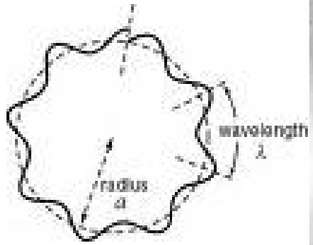

1986: E. Ruska
Nobel Prize

E. Ruska: 1931

The resolution limit of the light microscope due to the length of the light wave which had been recognized 50 years before by Ernst Abbe and others could, because of lack of light, not be important at such magnifications. Knoll and I simply hoped for extremely low dimensions of the electrons. As engineers we did not know yet the thesis of the “material wave” of the French physicist de Broglie that had been put forward several years earlier (1925). Even physicists only reluctantly accepted this new thesis. When I first heard of it in summer 1931, I was very much disappointed that now even at the electron microscope the resolution should be limited again by a wavelength (of the "Materiestrahlung"). I was immediately heartened, though, when with the aid of the de Broglie equation I became satisfied that these waves must be around five orders of magnitude shorter in length than light waves. Thus, there was no reason to abandon the aim of electron microscopy surpassing the resolution of light microscopy.

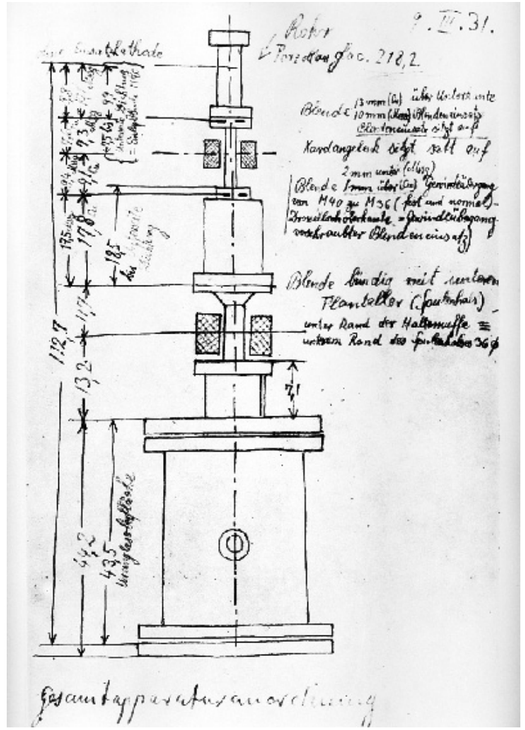

Electron Wavelengths in Electron Microscopes

Electron charge (e)	-1.602 x 10^{-19} C
1 eV	1.602 x 10^{-19} J
Electron rest mass (m_o)	9.109 x 10^{-31} kg
Electron rest energy ($m_o c^2$)	511 keV
Kinetic energy (charge x tension)	1.602 x 10^{-19} Nm (per 1 volt)
Plank's constant (h)	6.626 x 10^{-34} N-m-s
1 Ampere	1 C/sec
Light speed in vacuum (c)	2.998 x 10^{8} m/sec

non relativistic (<50keV)

$$\lambda = \frac{h}{(2m_0 eV)^{1/2}}$$

Relativistic correction

$$\lambda = \frac{h}{\left[2m_0 eV\left(1+\frac{eV}{2m_0 c^2}\right)\right]^{1/2}}$$

Accelerating voltage [KV]	Nonrelativistic λ [nm]	Relativistic λ [nm]	Mass [x m_o]	Velocity [x 10^8 m/s]
1	0.03879	0.03878	1.002	0.13
10	0.01227	0.01221	1.02	0.42
80	0.00434	0.00418	1.157	1.1
200	0.00274	0.00251	1.391	1.59
300	0.00224	0.00197	1.587	1.82
1000	0.00123	0.00087	2.957	2.44

Diffraction Limited Resolution

Raleigh's Criterion

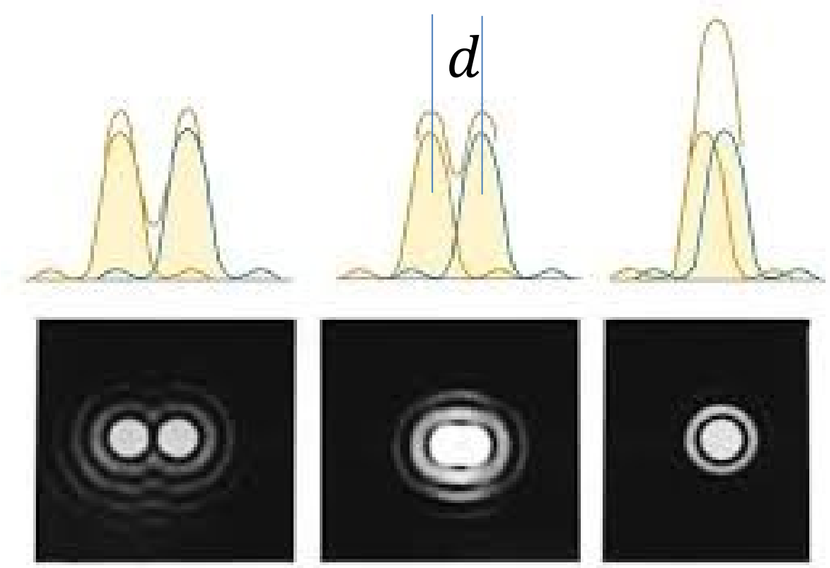

Airy Diffraction Disks

$$d = 0.61\frac{\lambda}{n\sin\theta} = 0.61\frac{\lambda}{\beta}$$

Green light : $\lambda \approx 532$ nm,

β (objective collection angle)~1 rad

n= 1.7 for oil immersion lens

*** d=200nm

Electrons 200 keV : $\lambda \approx 0.00251$nm

n=1 for vacuum

β=0.1 rad given TEM geometry

***d=0.015 nm

Aberration Correction

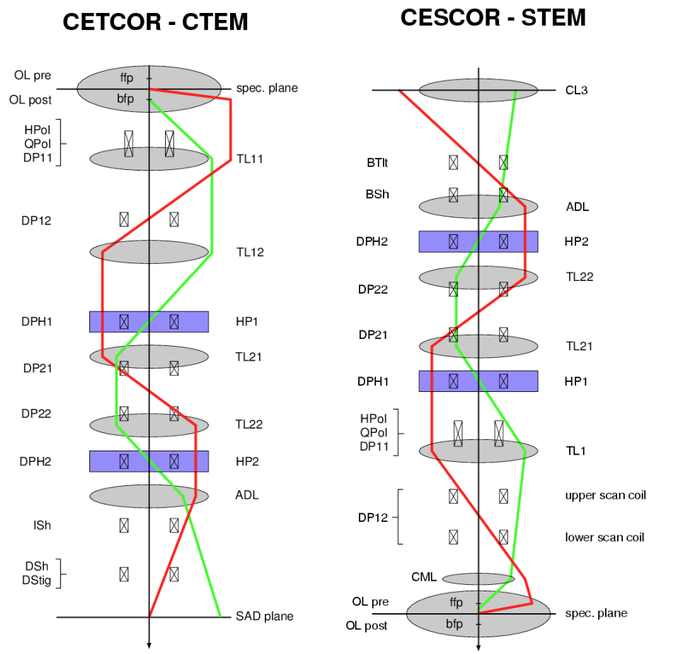

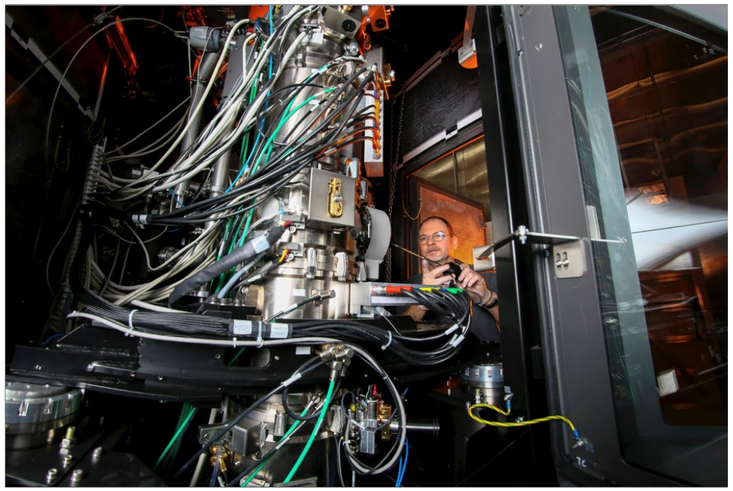

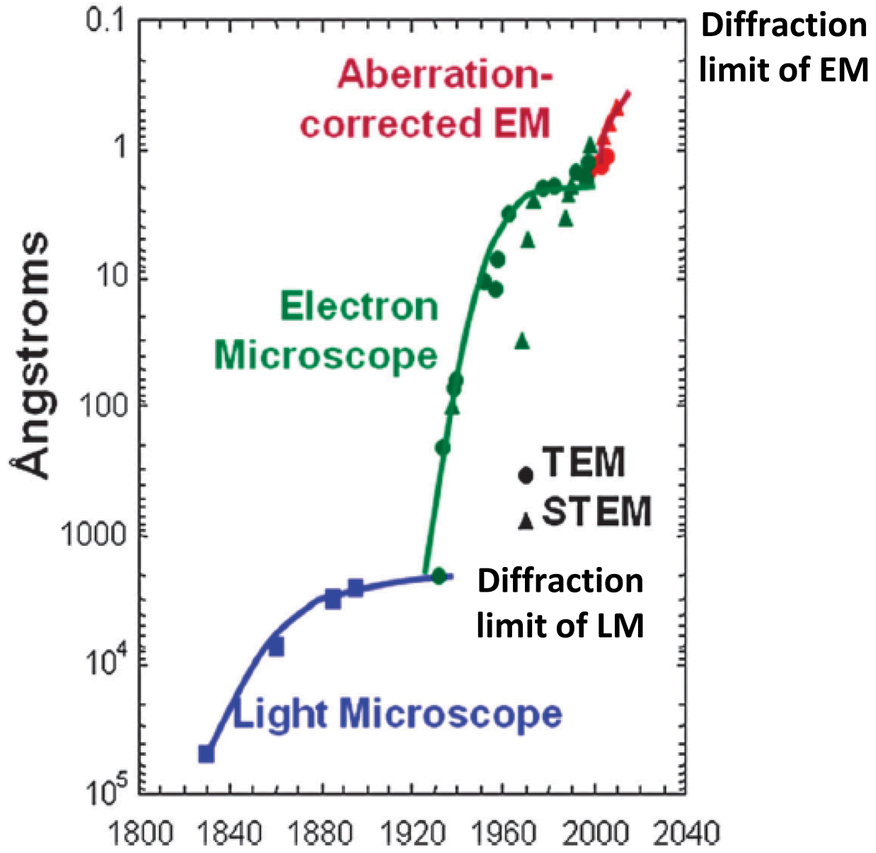

Uncorrected resolution is ~150 X diffraction limit

Cs-Corrected resolution is ~20 x diffraction limit

Transmission Electron Microscope

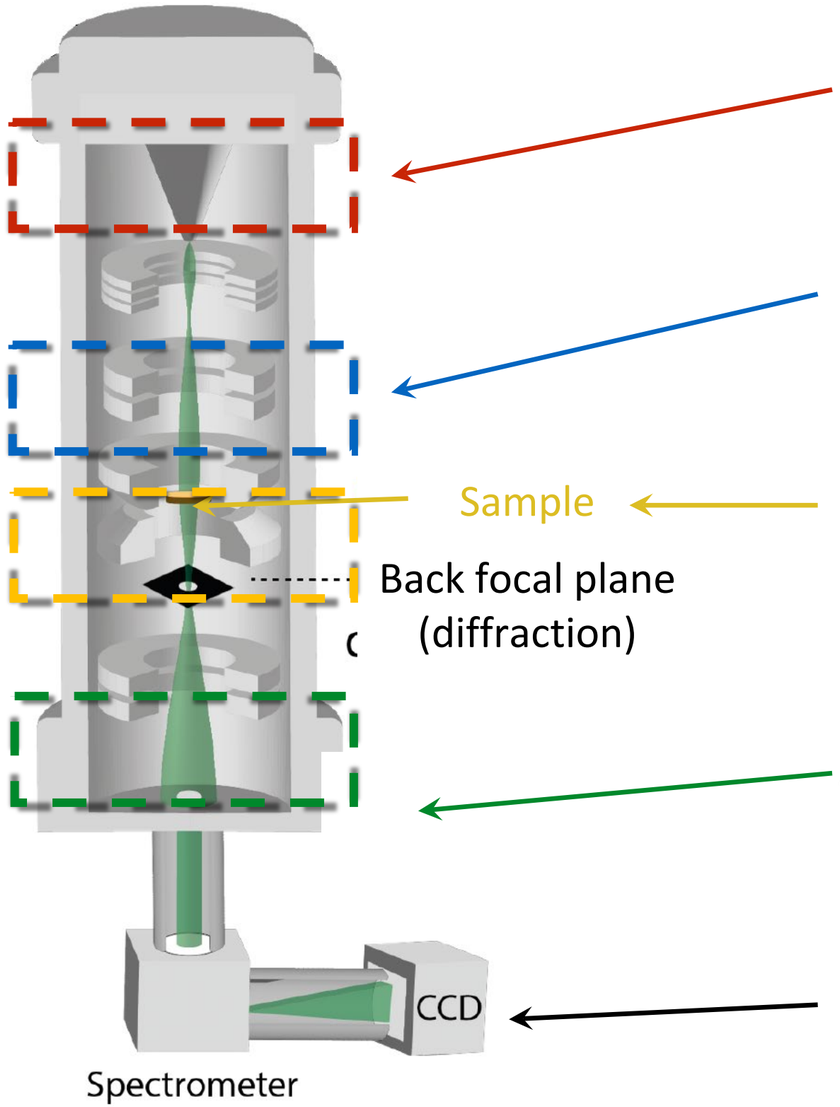

1. Gun – Thermionic or Field emission. Electrons are accelerated to different voltages (wavelengths)
2. Condenser lenses- changes spot size, illumination area, and convergence angle on the sample (forms STEM probes)
3. Objective lens – images the sample. The electron diffraction patterns are formed in the back focal plane, where the objective aperture is also located.
4. Intermediate lenses- changes modes from imaging to diffraction, magnification, and camera lengths
5. Detectors- cameras, STEM detectors, electron spectrometer

Interaction of high energy electrons with samples

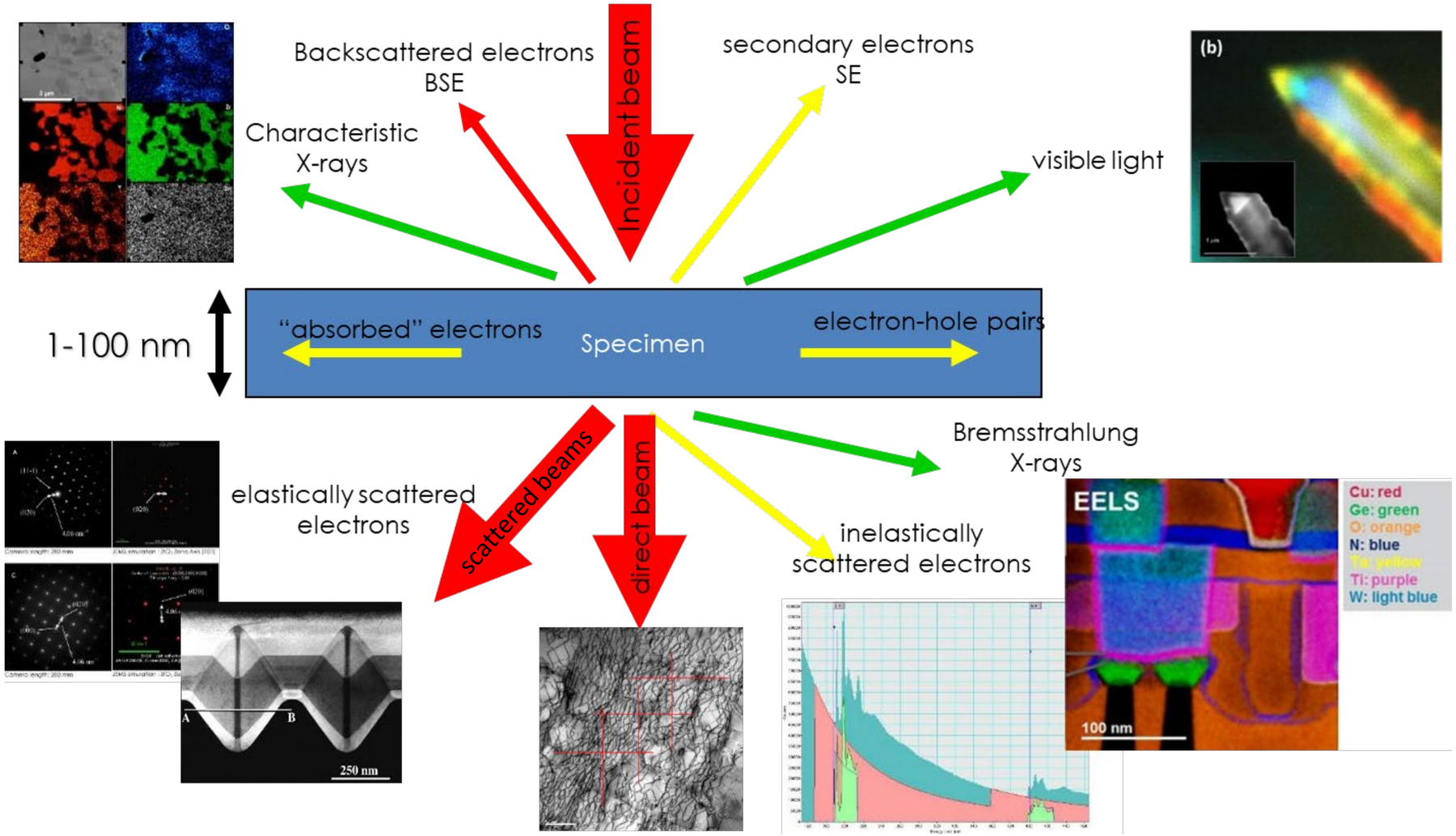

Selected Area Electron Diffraction

$$2dsin\theta = 2\theta d = n\lambda$$

$$R\lambda = 2\theta = R/CL, d_{hkl} = \lambda CL/R$$

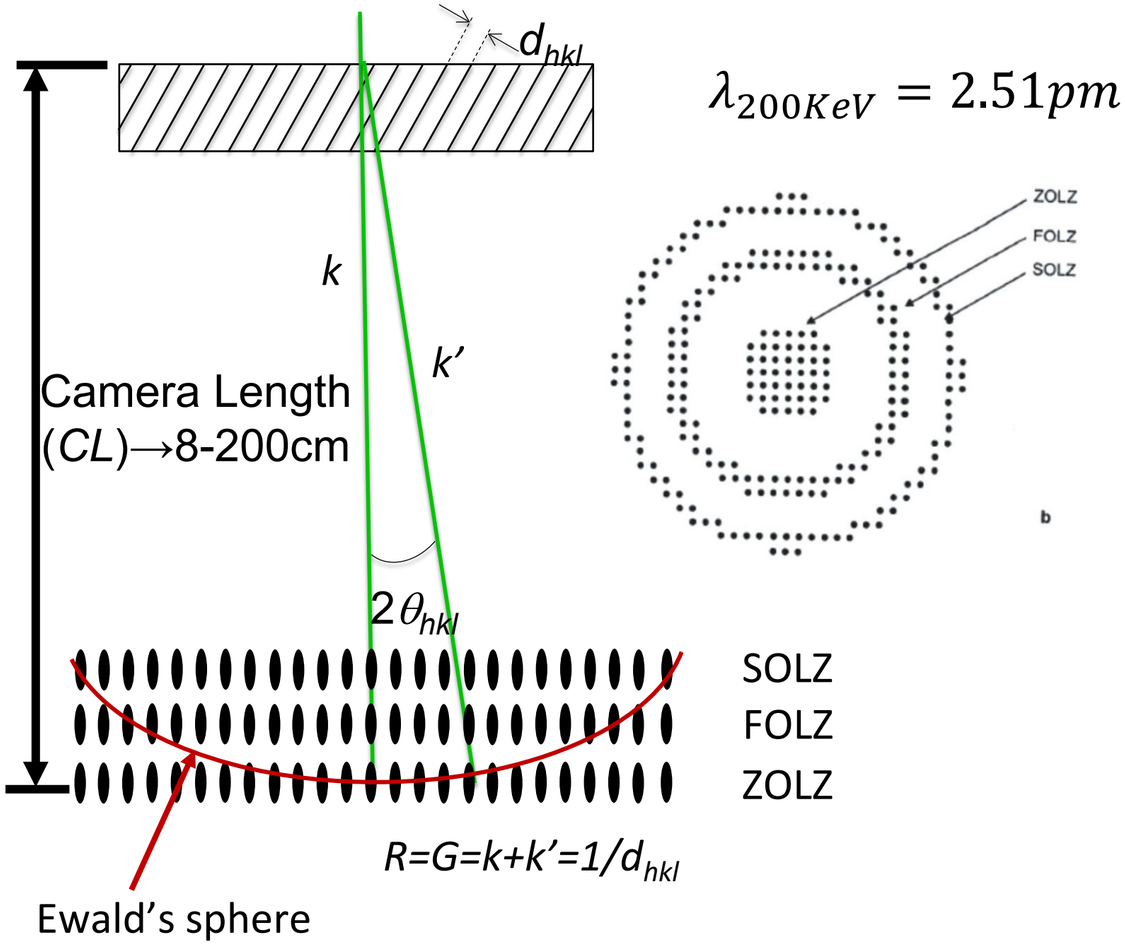

$$\lambda_{200KeV} = 2.51pm$$

Bragg Diffraction Powder Pattern

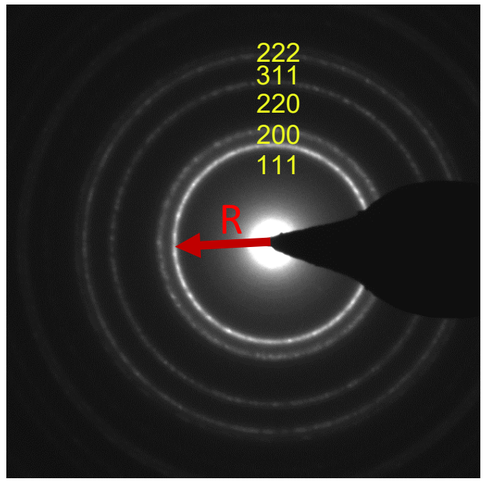

Single Crystal Spot Pattern

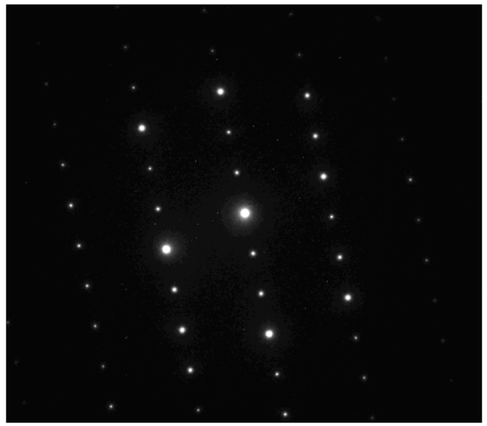

Ewald's Sphere and excitation error

a)

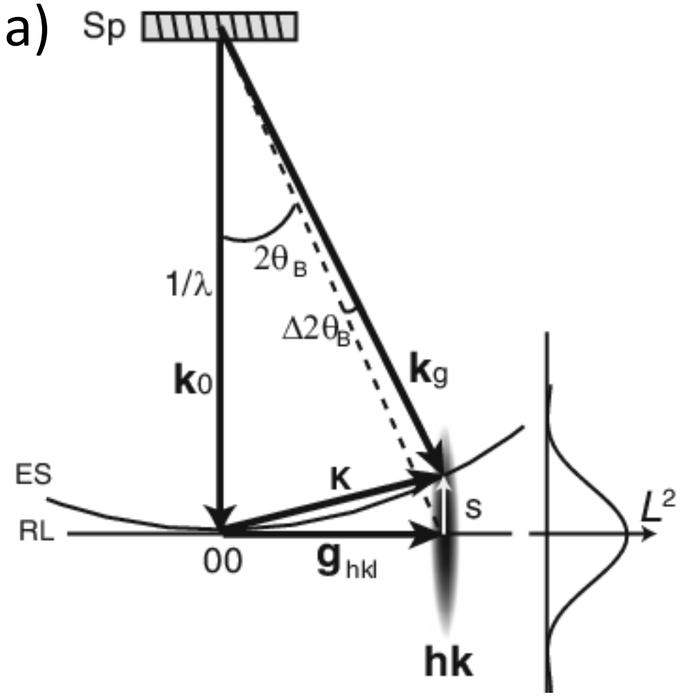

b)

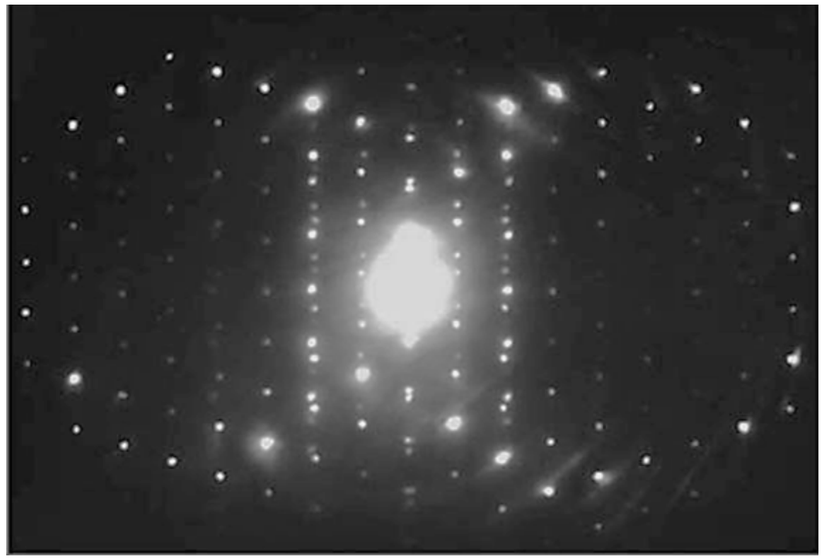

c)

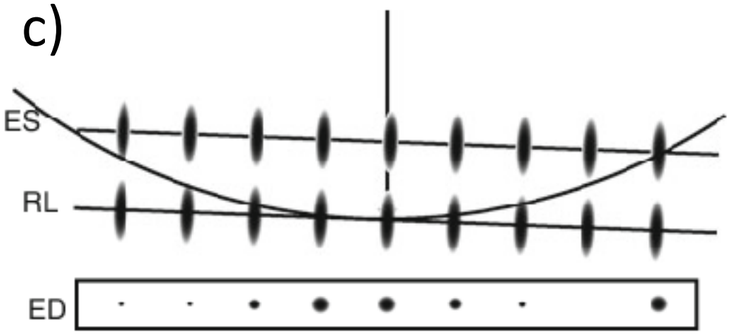

Excitation error (s),

$$k = g_{hkl} + s$$

Characteristic diffraction vector length, extinction distance

$$\xi_g = {\pi V_c cos\theta_B}\Big/{\lambda F_g}$$

2-Beam Condition

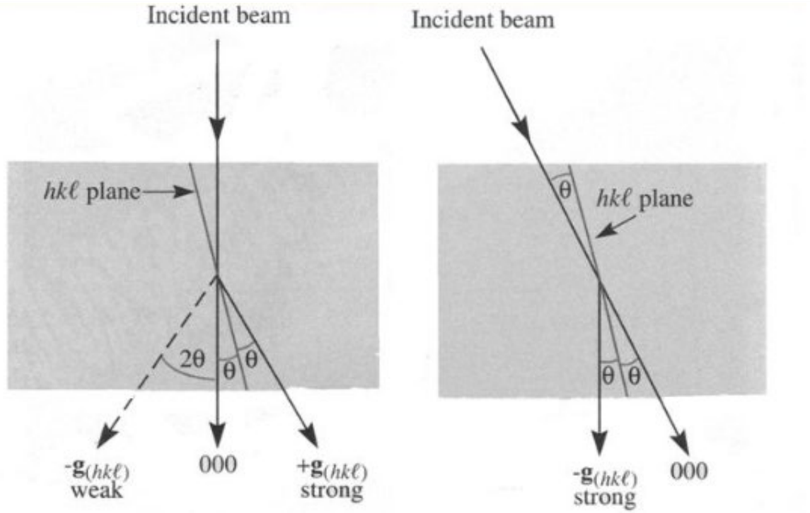

Brightfield

Darkfield

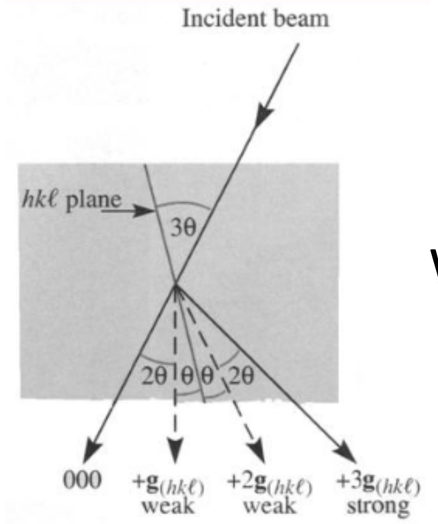

Weak-beam Darkfield

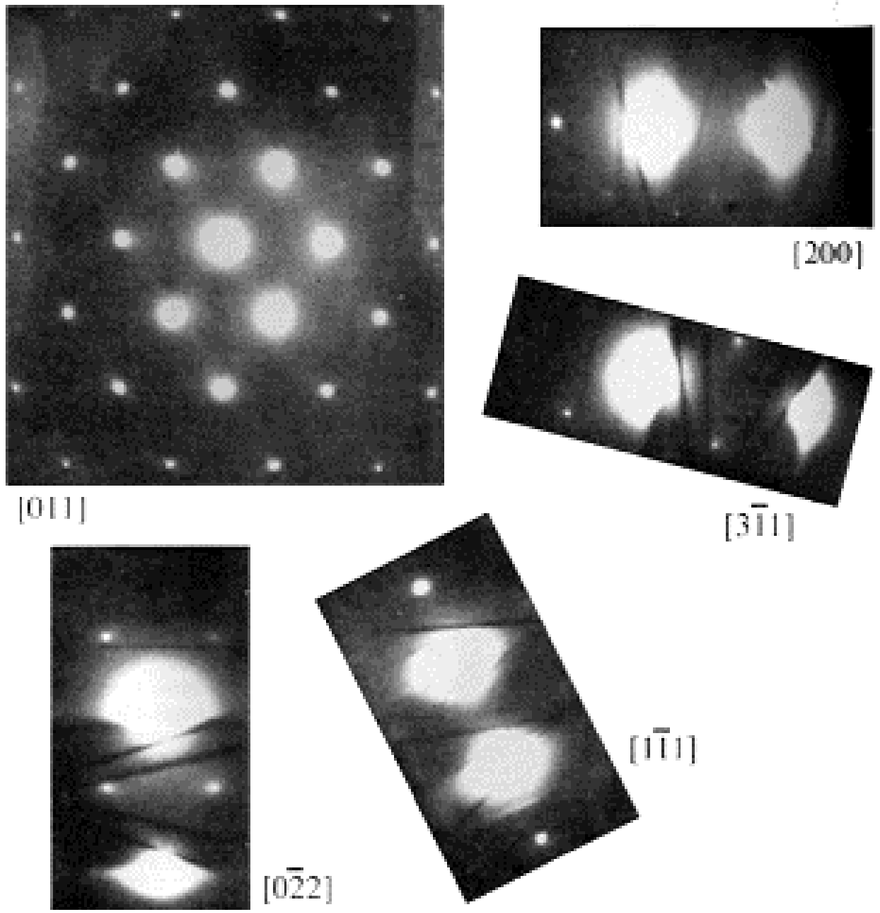

Diffraction Contrast

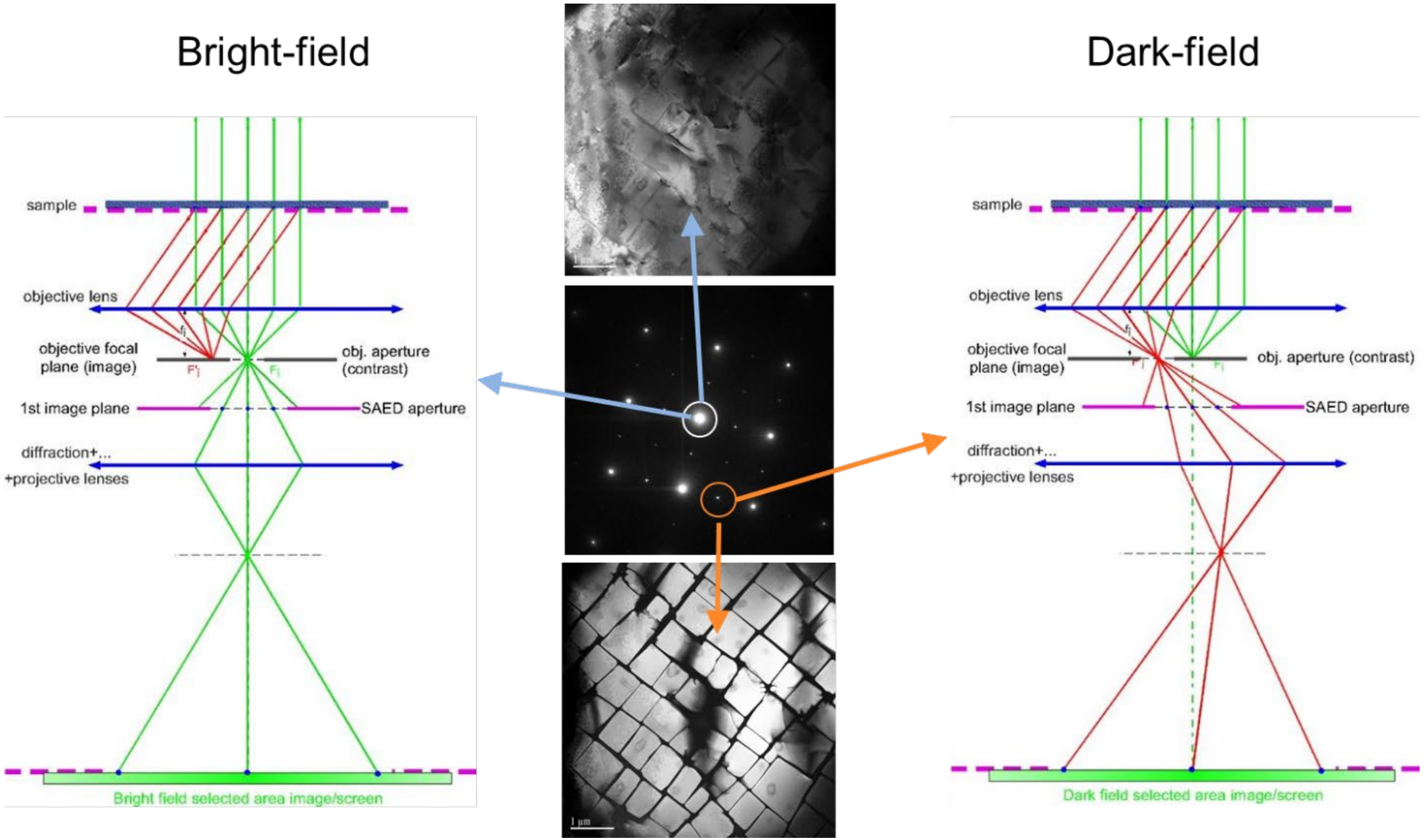

Dislocation imaging

- Strong beam Bright-field or Two beam condition: the sample is first tilted such that g image is excited (Ewald sphere intersects g) and strong in intensity.
- Strong beam Dark field: the image is formed using the excited, high-intensity (g) diffracted beam
- Weak Beam Dark-field (WBDF): the sample is tilted such that the 3g and 0 spots are both excited, and the objective aperture is centered on the **WEAK** g spot.

WBDF is useful for imaging defects since the excitation error is small, and defects such as dislocations are better resolved

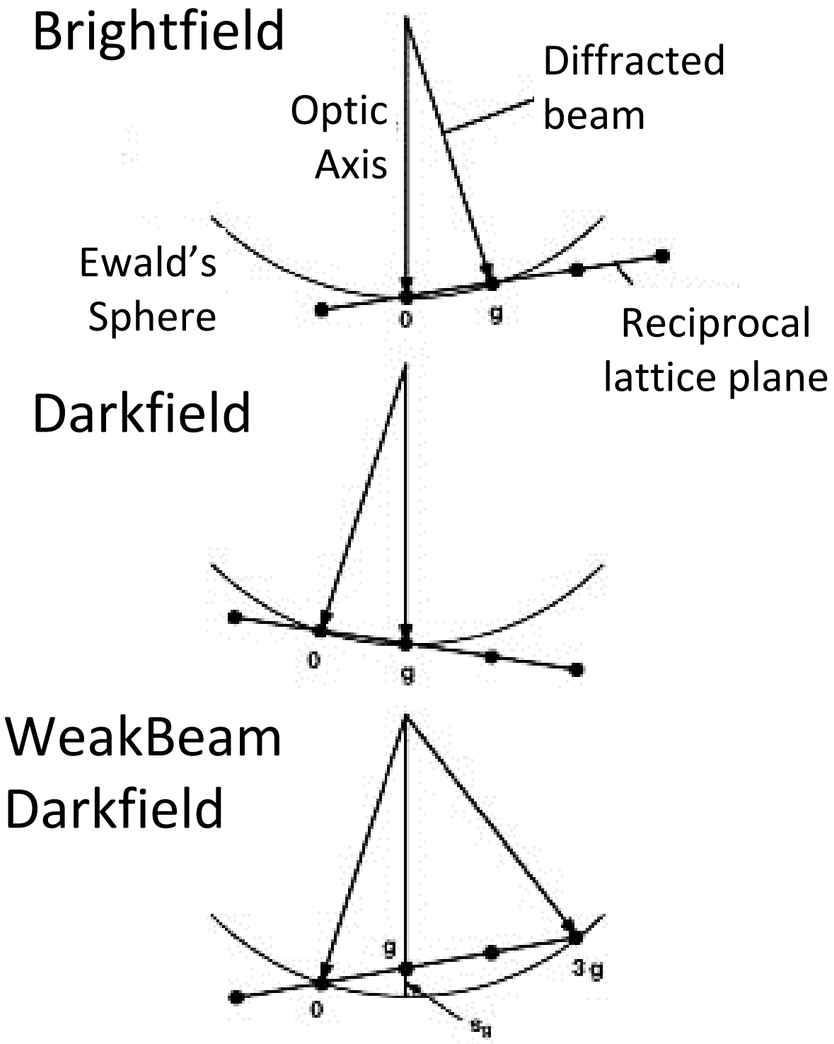

ZA (Kinematical) imaging vs. 2-Beam vs. Weak Beam

Zone Axis Bright-field

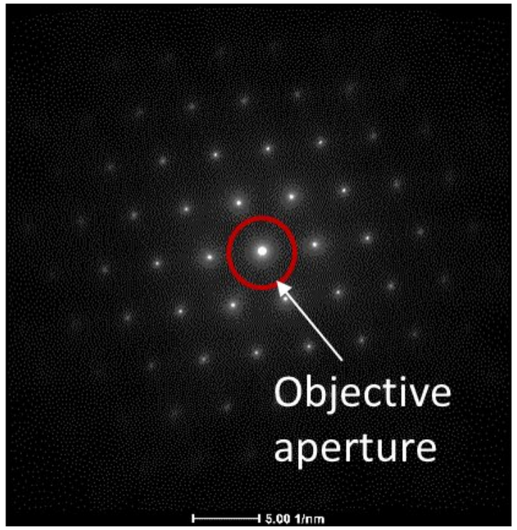

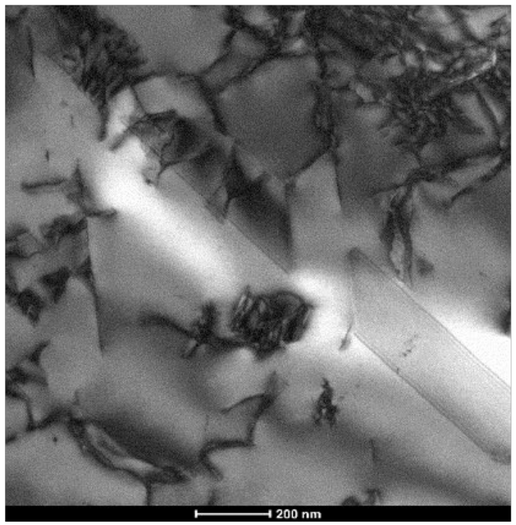

Two Beam Bright-field

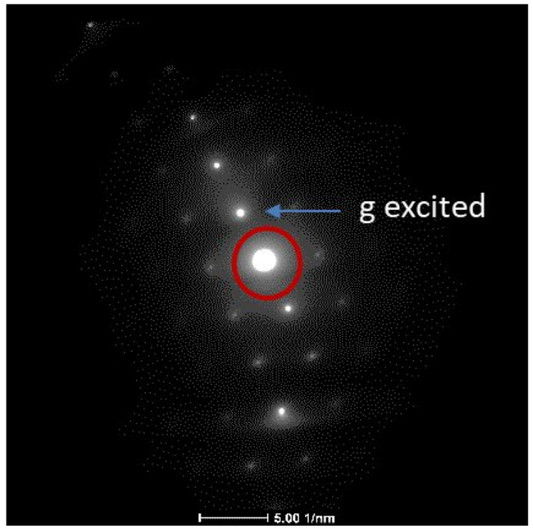

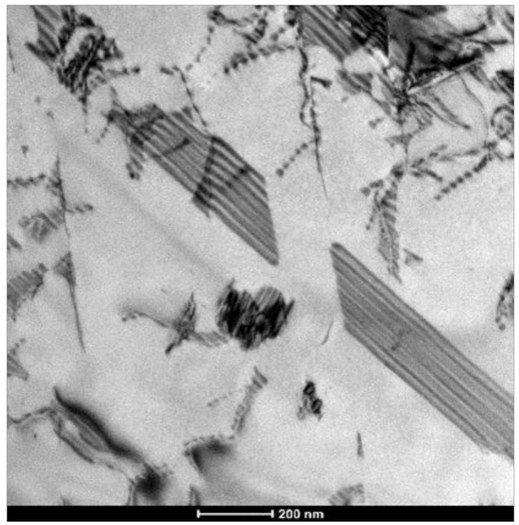

Weak Beam Image

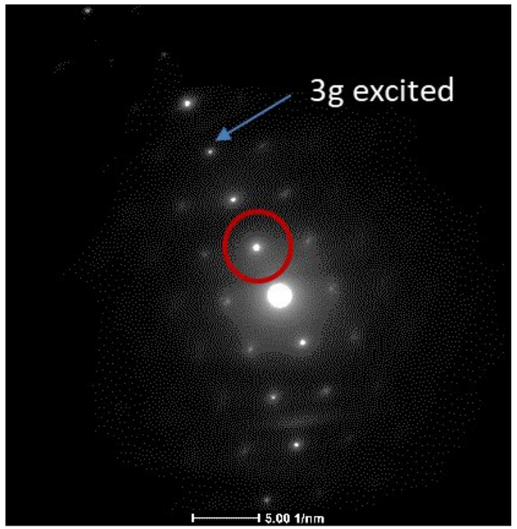

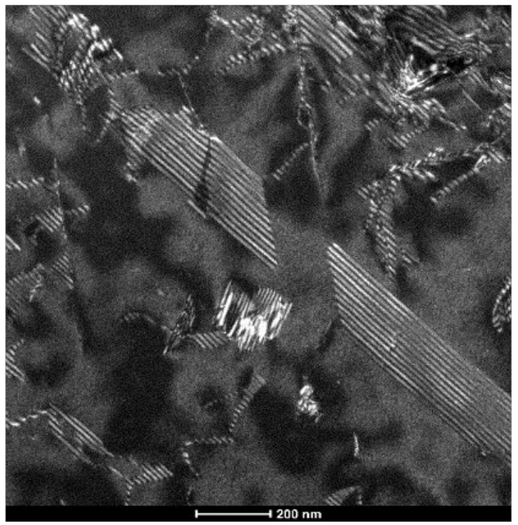

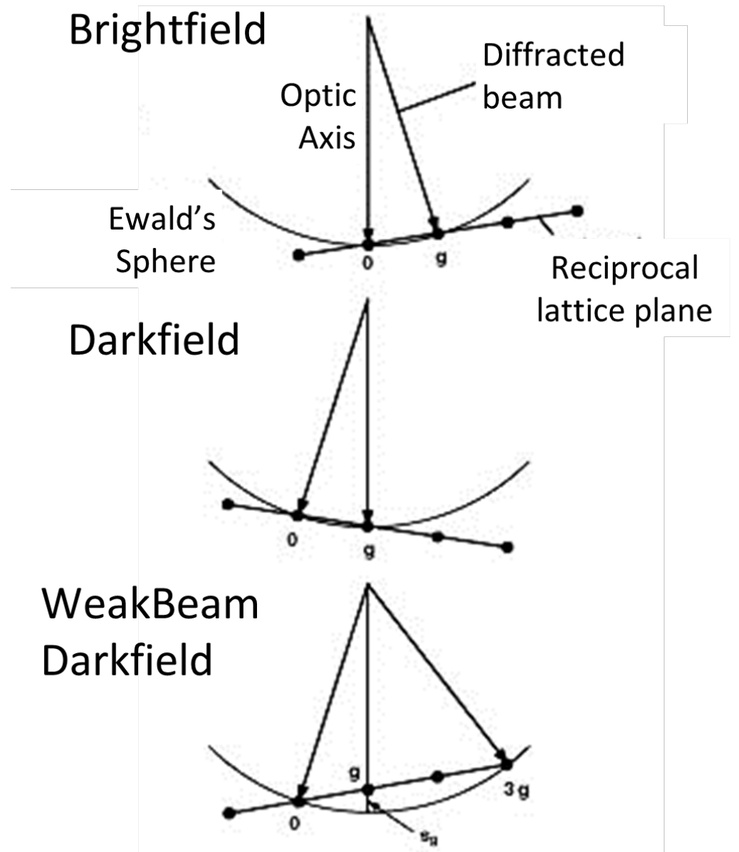

Stacking Faults imaged with Weak Beam

Two Beam Bright-field

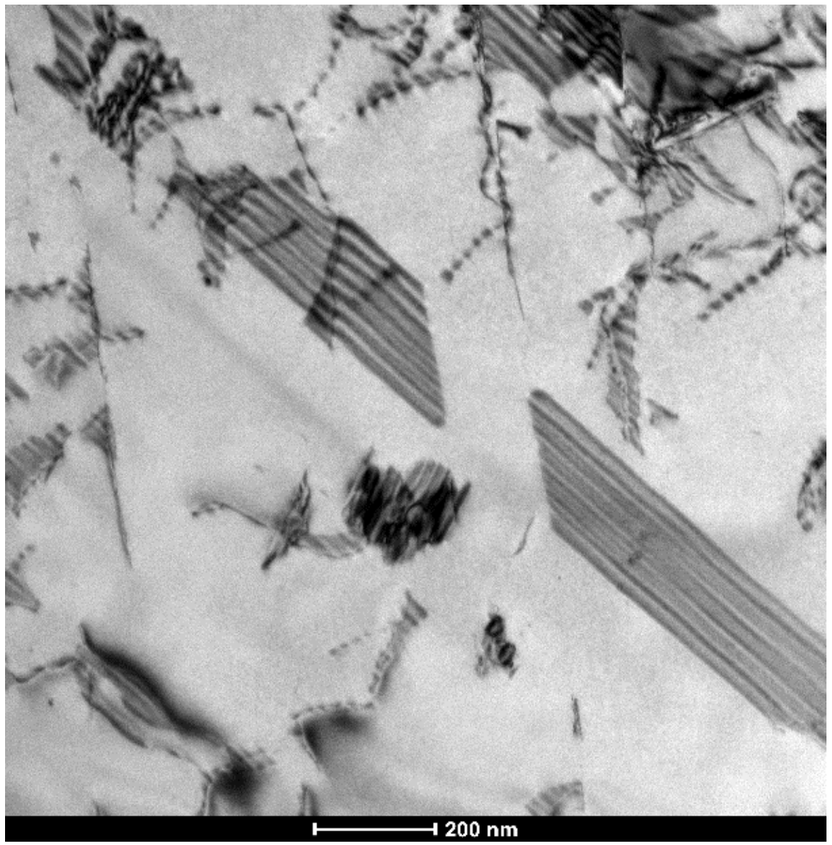

Weak Beam Image

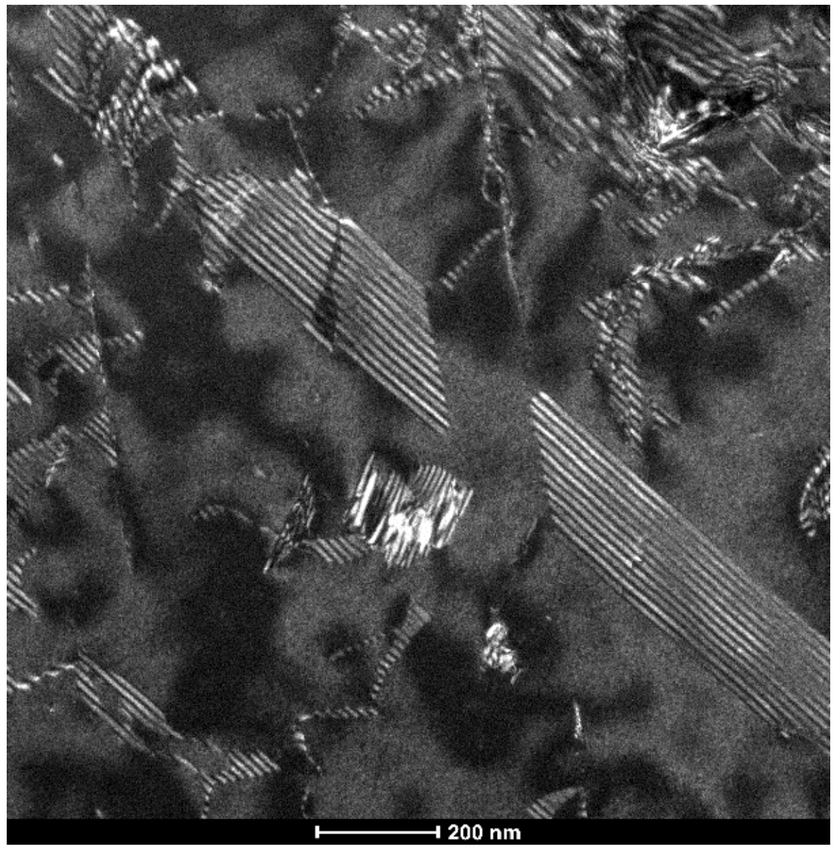

Fringe spacing correlates to partial dislocation separation distances which can be measured clearly in weak beam due to improved contrast and resolution

Weak-beam provides <5nm resolution

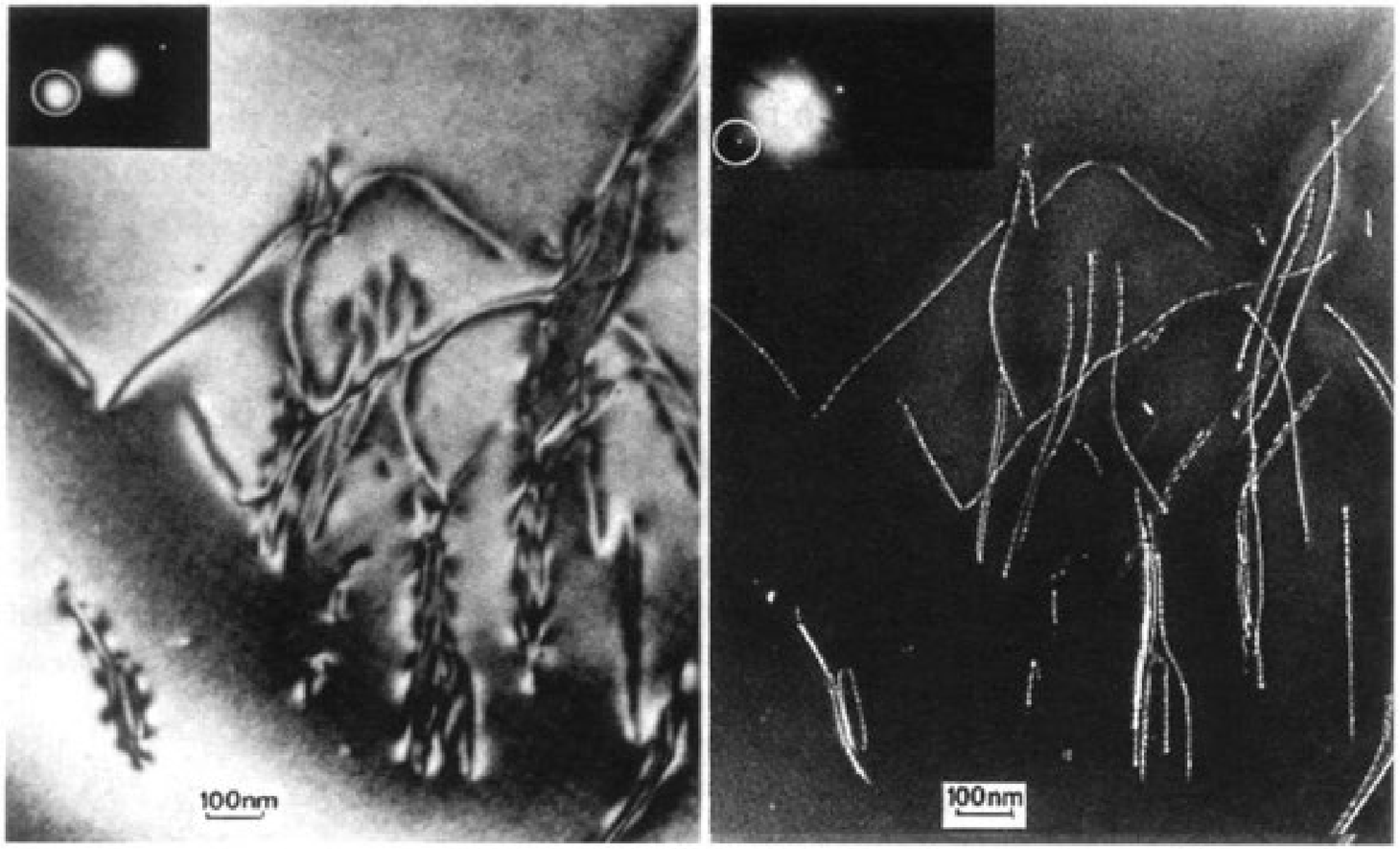

Kinematical Diffraction

Assumptions

- Only 2 diffracted beams are considered, direct and one diffracted (aka why we do 2-beam condition)
- Intensity of the diffracted beam is small
- Single scattering event, that is “one cycle” intensity change
- No absorption, i.e., $I_{diffracted} << I_{transmitted}$

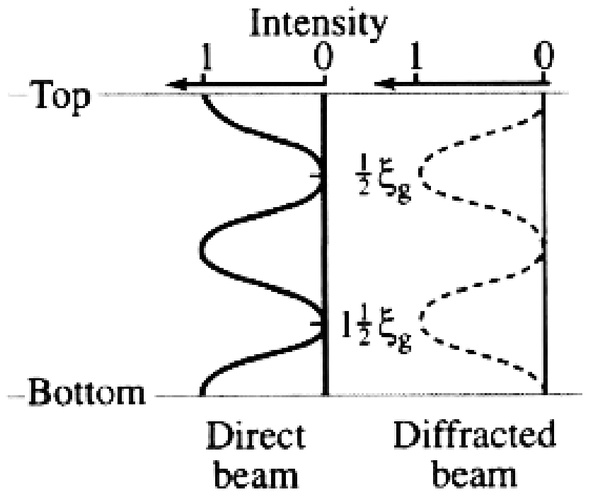

$$I_{diff} = \frac{sin^2(\pi z s)}{\xi_g s^2}$$

$$I_{trans} = 1 - I_{diff}$$

$$\xi_g = {\pi V_c cos\theta_B}\Big/{\lambda F_g}$$

Thickness Fringes

Brightfield

Darkfield

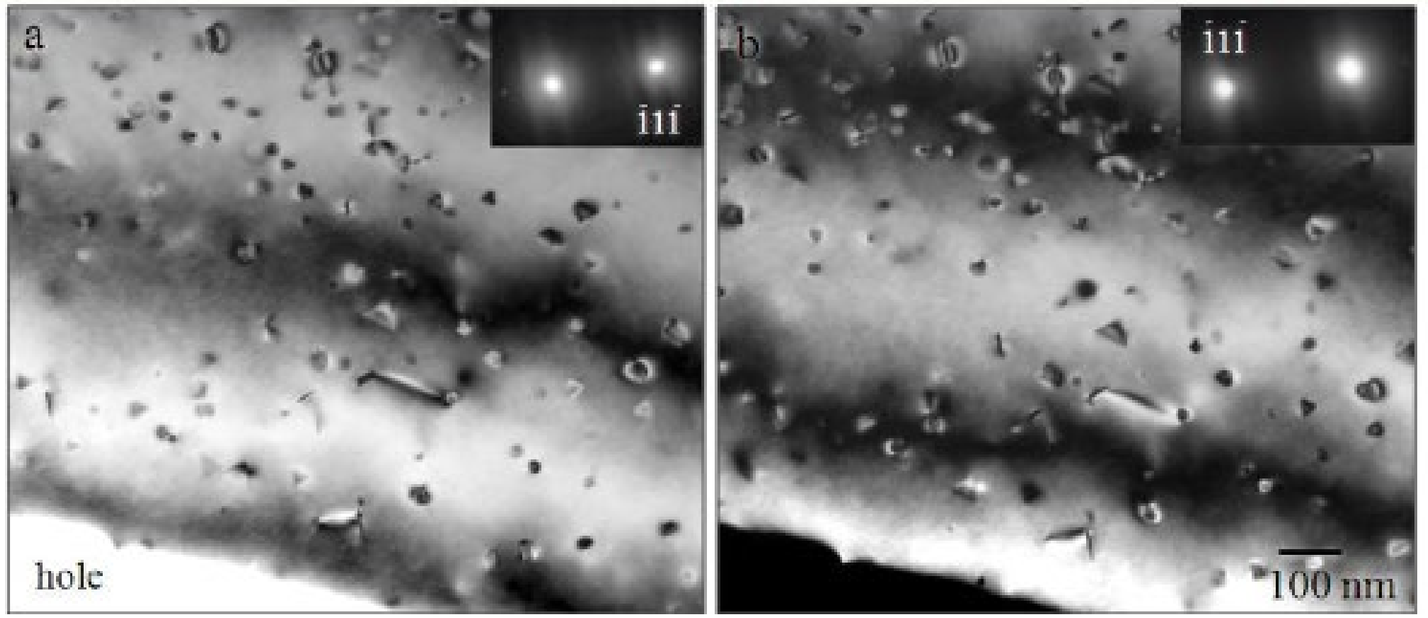

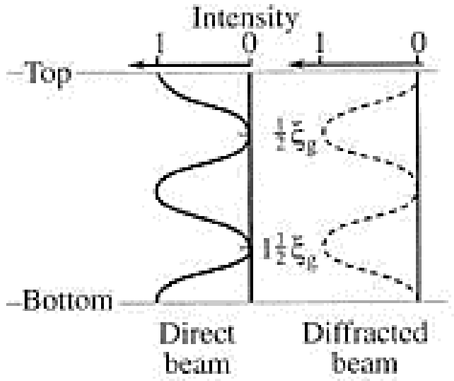

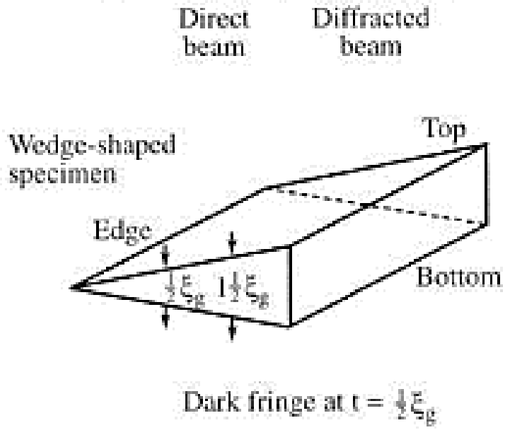

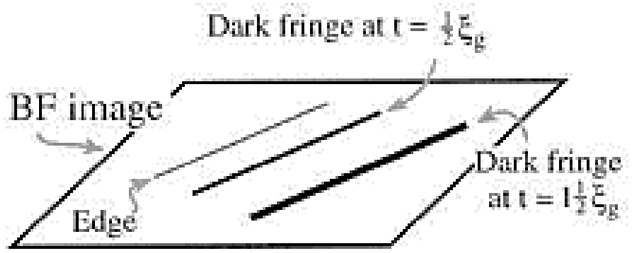

Bend Contours

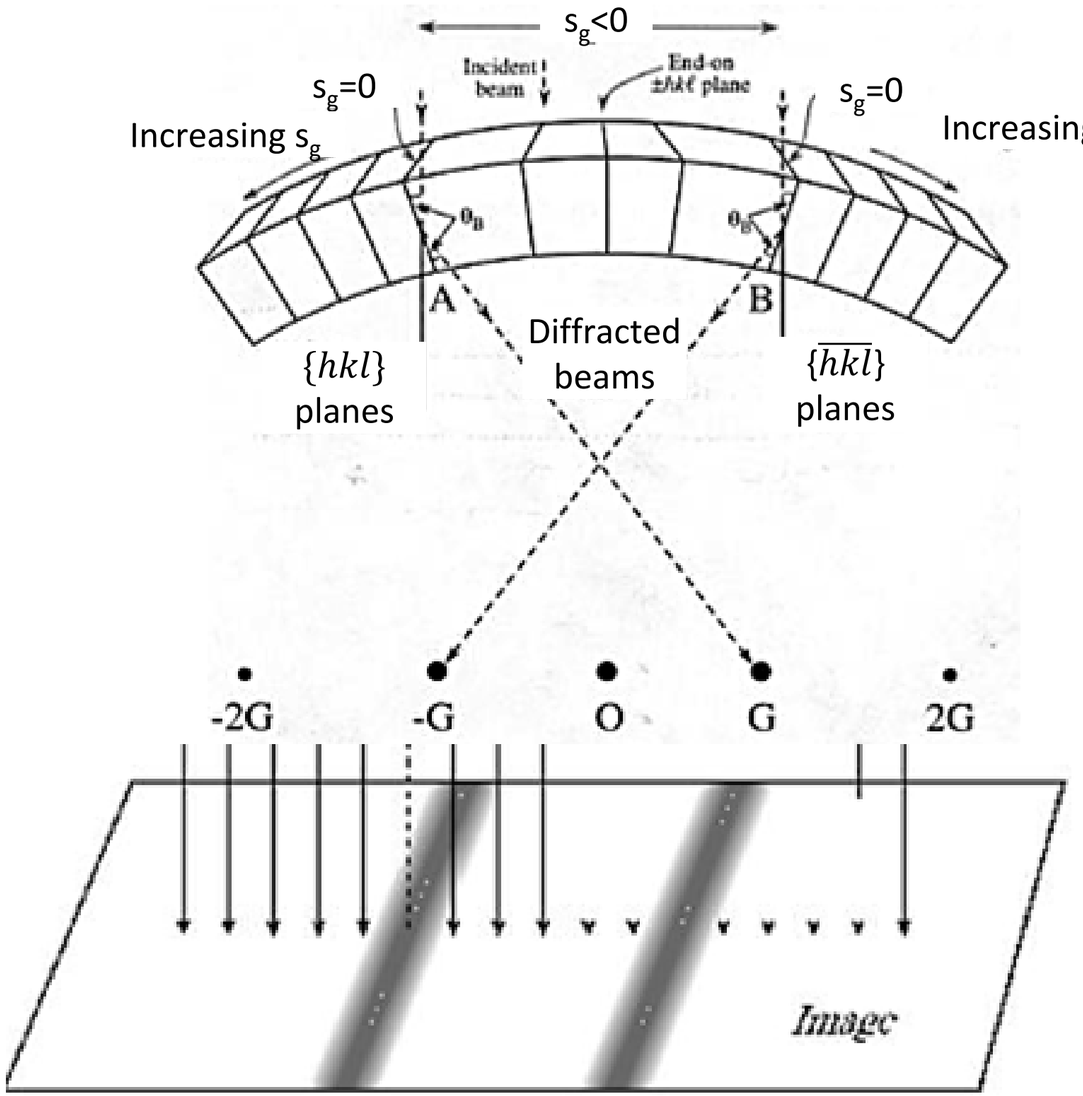

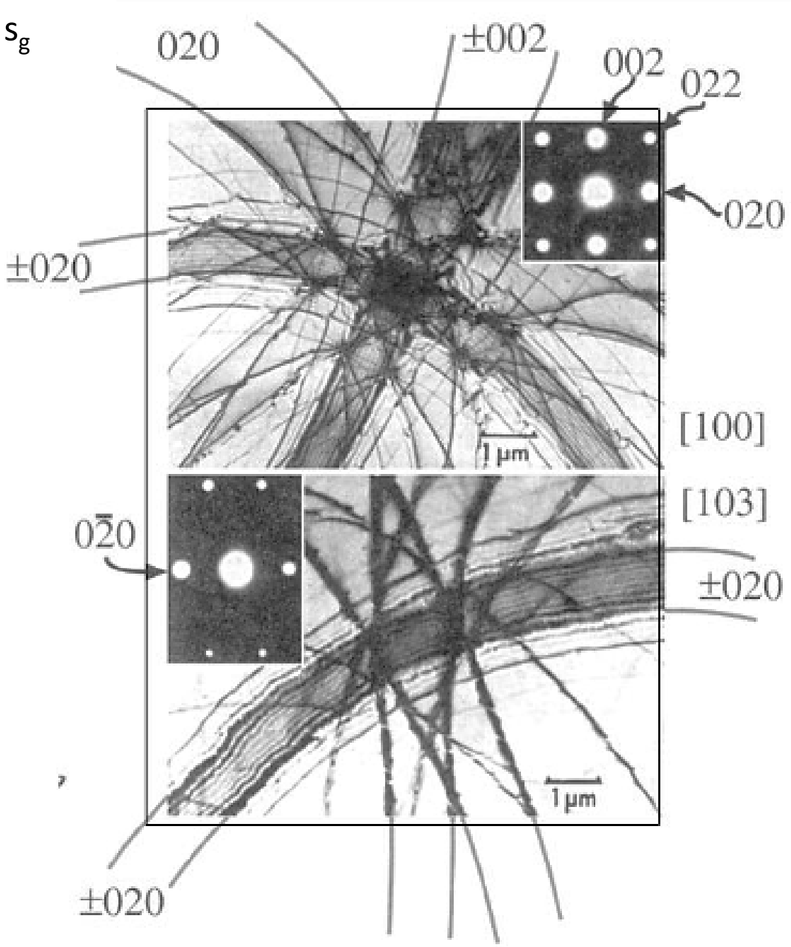

Kinematic Diffraction in crystals with defects

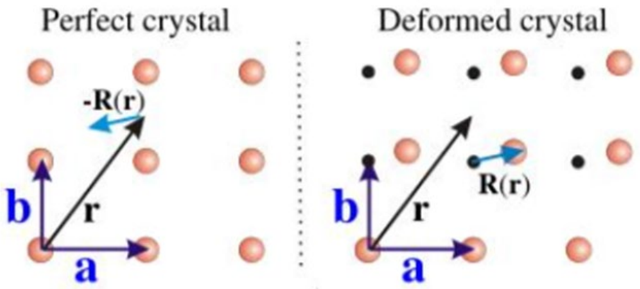

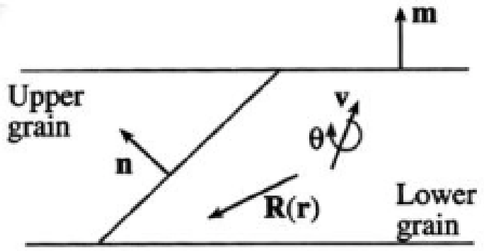

$$V_{def}(r) = \sum_g V_g e^{2\pi i \boldsymbol{g}\cdot[\boldsymbol{r}-\boldsymbol{R}(\boldsymbol{r})]}$$

Translations and rotations between two crystals produce fringes in the images

- Stacking Faults
- Grain boundaries
- Translation boundaries
- Phase boundaries
- Stepped Surfaces

Electron wave has different amplitude and phase in each crystal resulting in constructive –destructive interference and fringe patterns

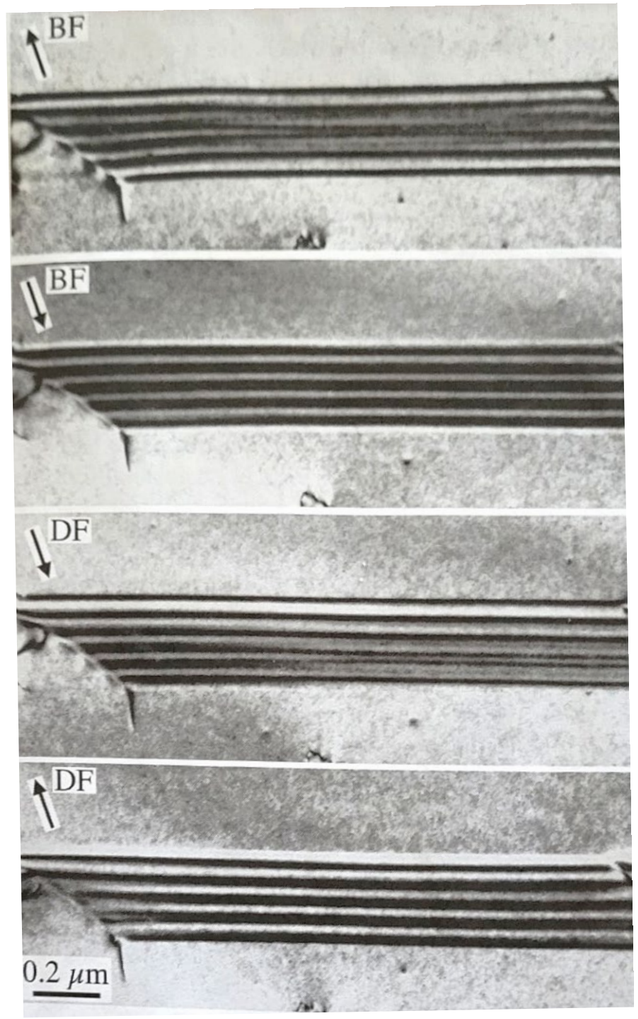

Howie Whelan Equations

$$V(r) = \sum_g V_g e^{2\pi i \boldsymbol{g}\cdot r}$$

Potential of perfect crystal

$$A_{cell} = \frac{e^{2\pi i \boldsymbol{k}\cdot\boldsymbol{r}}}{r} F(\theta)$$

Electron scattering amplitude from a unit cell

$$\phi_g = \frac{\pi a i}{\xi_g} e^{2\pi i \boldsymbol{K}\cdot\boldsymbol{r_a}} e^{2\pi i \boldsymbol{k}_g\cdot\boldsymbol{r}}$$

Scattering amplitude of a diffracted beam (solved using Schrödinger's eqn.)

$$\Psi_T = \phi_o e^{2\pi i \boldsymbol{k}_o\cdot\boldsymbol{r}} + \phi_{g1} e^{2\pi i \boldsymbol{k}_{g1}\cdot\boldsymbol{r}} + \phi_{g2} e^{2\pi i \boldsymbol{k}_{g2}\cdot\boldsymbol{r}} + \phi_{g3} e^{2\pi i \boldsymbol{k}_{g3}\cdot\boldsymbol{r}} \ldots$$

Total wavefunction 2-beam condition

$$\phi_o = C_o e^{2\pi i \gamma z}, \quad \phi_g = 2\xi_g \gamma C_o e^{2\pi i \gamma z}$$

Scattering amplitudes in terms of γ phase, and ***r*** and ***s*** are parallel to ***z***

$$I_g = |\phi_g|^2$$

Solving the Bloch Wave equations gives I_{diff}

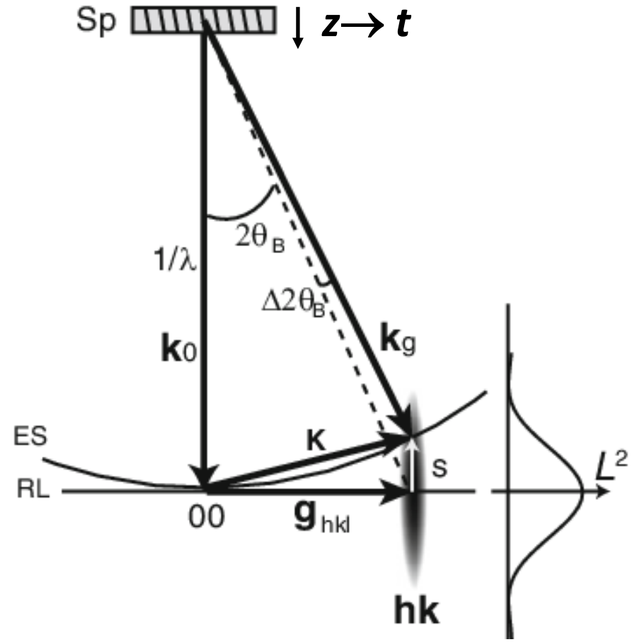

Extinction Distance

$$\xi_g = {\pi V_c \cos\theta_B} \Big/ {\lambda F_g}$$

Diffracted Intensity

$$I_g = \frac{\sin^2(\pi t s)}{\xi_g s^2}$$

$$I_o = 1 - I_g$$

Howie Whelan (Darwin) Equations

DYNAMICAL DIFFRACTION

The amplitudes of ϕ_g and ϕ_o are coupled and change with propagation in the sample.

$$d\phi_o = \left\{\frac{\pi i}{\xi_g}\phi_{\boldsymbol{g}} e^{-2\pi i \boldsymbol{K}\cdot\boldsymbol{r}} + \frac{\pi i}{\xi_o}\phi_o\right\} dz \text{ and } d\phi_g = \left\{\frac{\pi i}{\xi_g}\phi_{\boldsymbol{o}} e^{2\pi i \boldsymbol{K}\cdot\boldsymbol{r}} + \frac{\pi i}{\xi_o}\phi_g\right\} dz$$

HOWIE-WHELAN EQUATIONS (perfect crystal)

$$\frac{d\phi_o}{dz} = \left\{\frac{\pi i}{\xi_g}\phi_{\boldsymbol{g}} e^{2\pi i \boldsymbol{sz}} + \frac{\pi i}{\xi_o}\phi_o\right\} \text{ and } \frac{d\phi_g}{dz} = \left\{\frac{\pi i}{\xi_g}\phi_{\boldsymbol{o}} e^{-2\pi i \boldsymbol{sz}} + \frac{\pi i}{\xi_o}\phi_g\right\}, sz = \boldsymbol{s}\cdot\boldsymbol{r}$$

HOWIE-WHELAN EQUATIONS for DEFECTS

$$\phi_o(z)' = \phi_o \exp\left(\frac{-\pi i z}{\xi_o}\right)$$

$$\phi_g(z)' = \phi_g \exp\left(2\pi i s z - \frac{\pi i z}{\xi_o} + 2\pi i \boldsymbol{g}\cdot\boldsymbol{R}(\boldsymbol{r})\right)$$

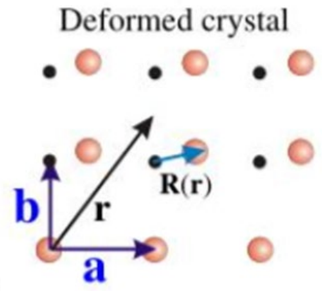

$$\frac{d\phi_g}{dz} = \frac{\pi i}{\xi_g}\phi_o(z)' + 2\pi i s_R \phi_g(z)' \text{ and } s_R = s + \boldsymbol{g}\cdot\frac{\boldsymbol{dR}(\boldsymbol{r})}{dz}$$

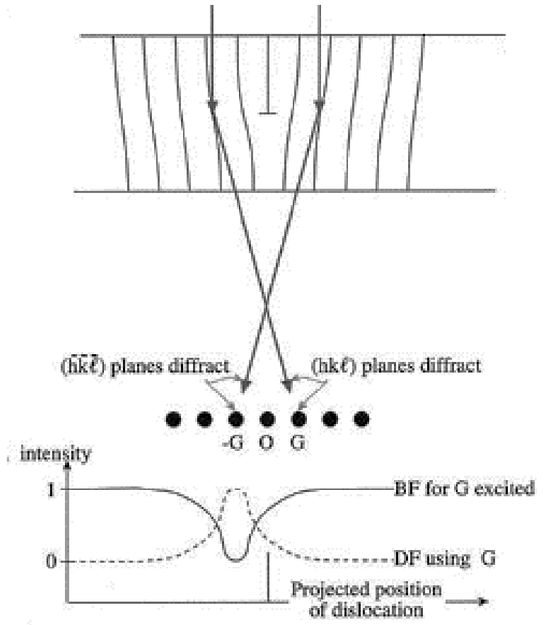

Strain Contrast for Dislocations

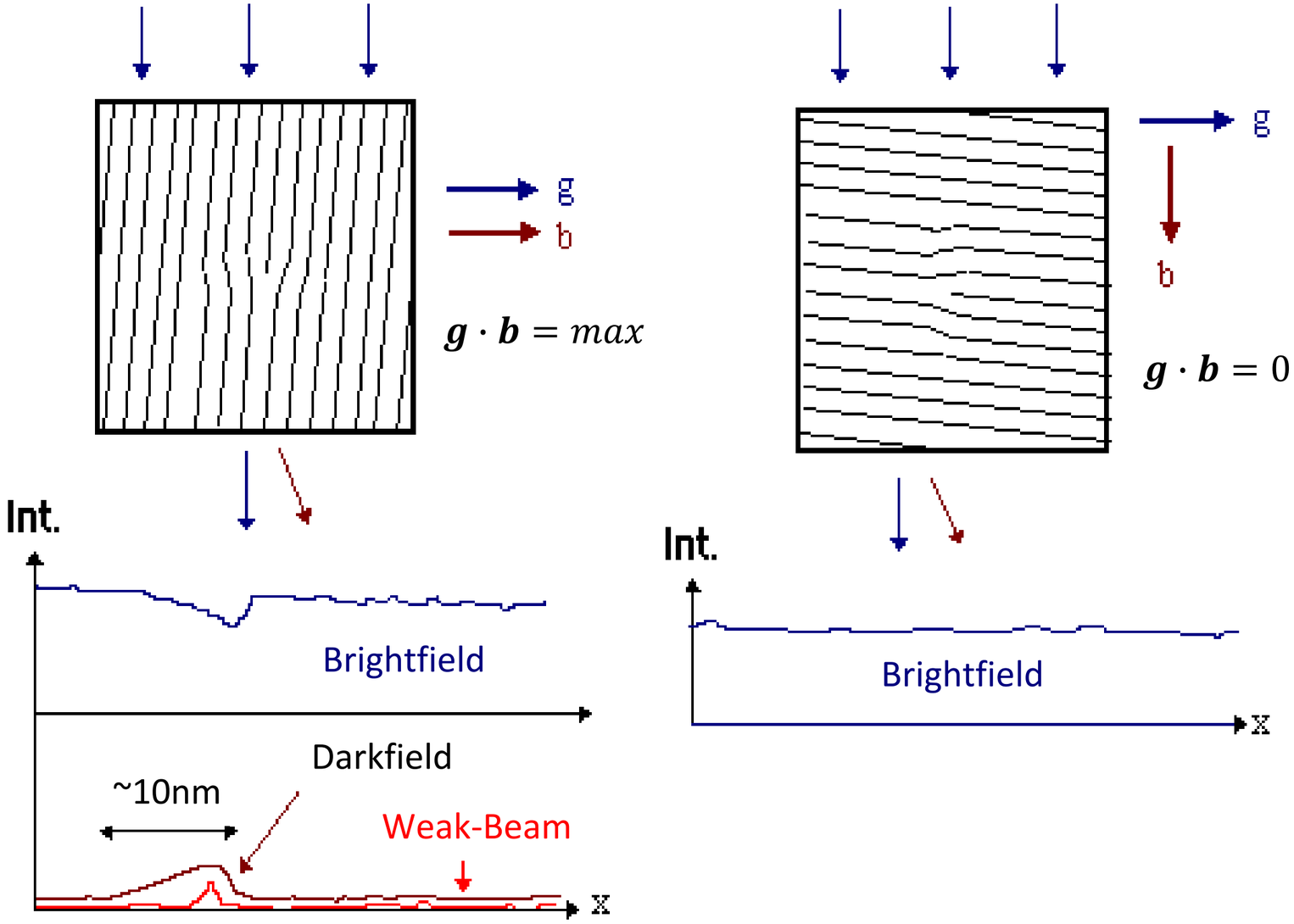

Invisibility Criterion of Screw Dislocations

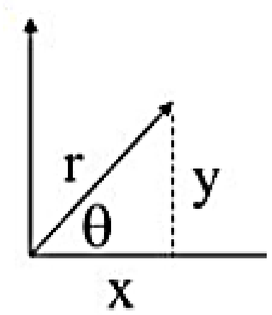

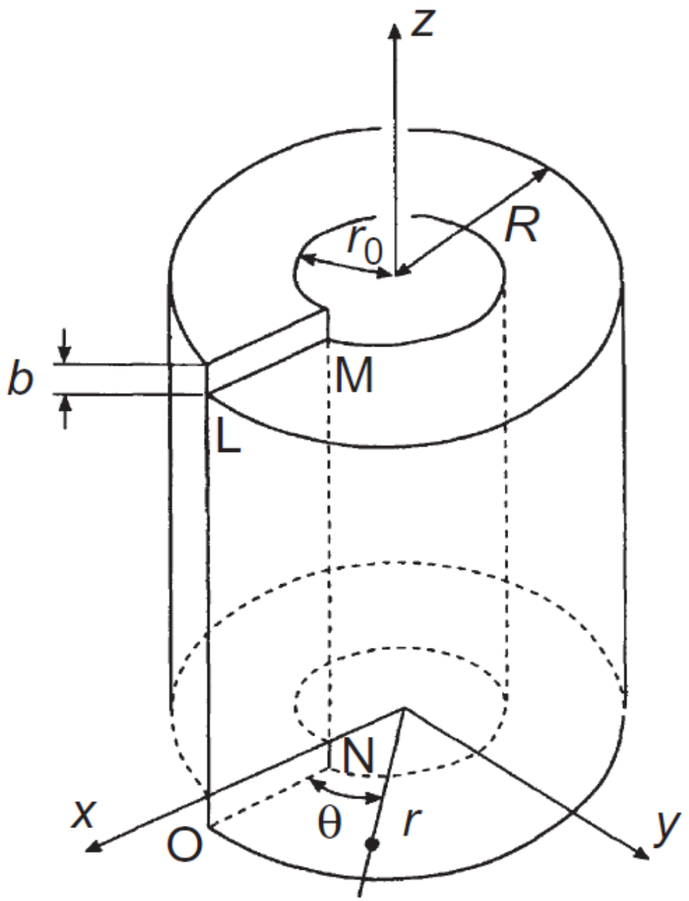

Shear Deformation along z directions on (r,z) plane

$$u_r = u_\theta = 0 \qquad u_z = \frac{b\theta}{2\pi}$$

$$R(x,y) = \frac{\boldsymbol{b}}{2\pi} tan^{-1}\left(\frac{x}{y}\right)$$

The contrast extinction condition require

$$\boldsymbol{g} \cdot \boldsymbol{R} = 0, \pm 1, \ldots \rightarrow \boldsymbol{g} \cdot \boldsymbol{b} = \boldsymbol{0}$$

Invisibility criterion for edge dislocation (isotropic)

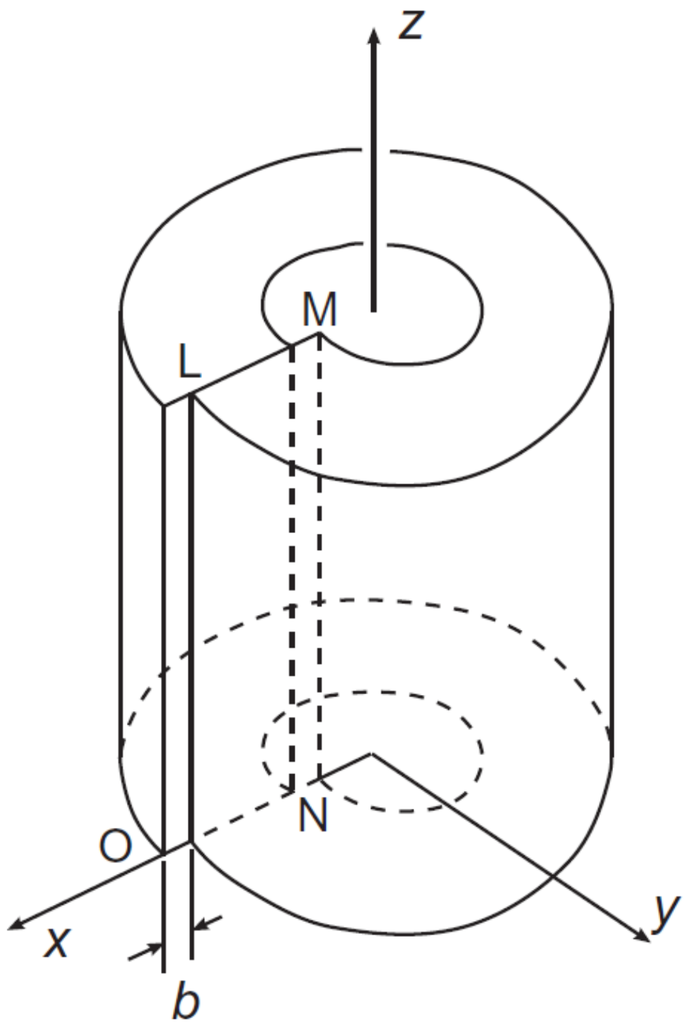

Plane Strain of edge dislocation

$$u_z = 0 \qquad u_x = \frac{b}{2\pi}\left(\theta + \frac{\sin 2\theta}{4(1-\nu)}\right)$$

$$u_y = -\frac{b}{2\pi}\left(\frac{1-2\nu}{2(1-\nu)}\ln r + \frac{\cos 2\theta}{4(1-\nu)}\right)$$

$$\boldsymbol{R} = \boldsymbol{b}\frac{\sin 2\theta}{4(1-\nu)} + \boldsymbol{b}\Lambda\vec{\boldsymbol{\xi}}\left(\frac{1-2\nu}{2(1-\nu)}lnr + \frac{\cos 2\theta}{4(1-\nu)}\right)$$

The contrast extinction condition requires

$$\boldsymbol{g}\cdot\boldsymbol{R} = 0, \pm 1, \ldots \rightarrow \boldsymbol{g}\cdot\boldsymbol{b} = \boldsymbol{0}$$

$$\boldsymbol{g}\cdot(\boldsymbol{b}\Lambda\overrightarrow{\boldsymbol{\xi}}) = 0 \ldots \rightarrow \boldsymbol{g} \parallel \vec{\boldsymbol{\xi}}\cdot\boldsymbol{b} = \boldsymbol{0}$$

Burger's vector determination

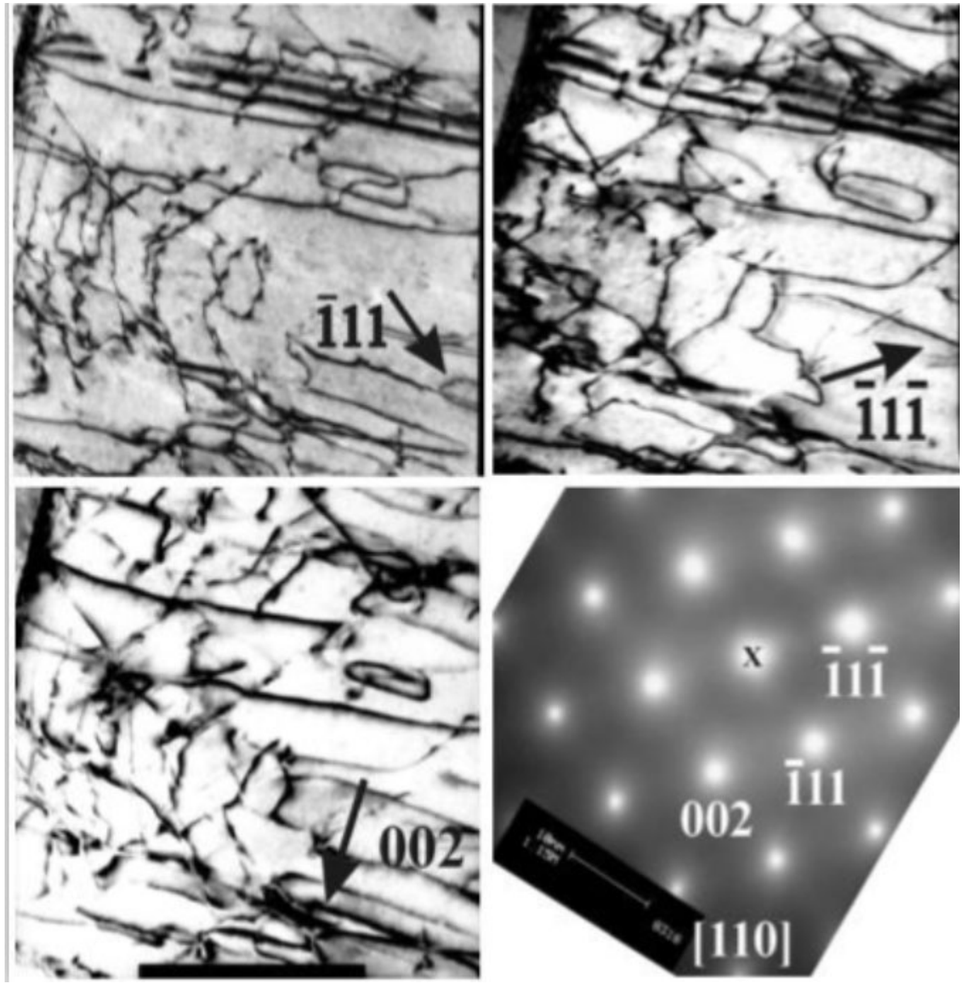

g	b	$g \cdot b$	$g \cdot b \wedge \vec{\xi}$
$[\bar{1}11]$	$1/2[110]$	0	$\neq 0$
	$1/2[0\bar{1}1]$	0	$\neq 0$
	$1/2[101]$	0	$\neq 0$
$[\bar{1}11]$	$1/2[1\bar{1}0]$	-1	$\neq 0$
	$1/2[011]$	-1	$\neq 0$
	$1/2[10\bar{1}]$	-1	$\neq 0$

Possible Burger's vectors
$[0\bar{1}1]$ and $[101]$

Stacking Fault Contrast

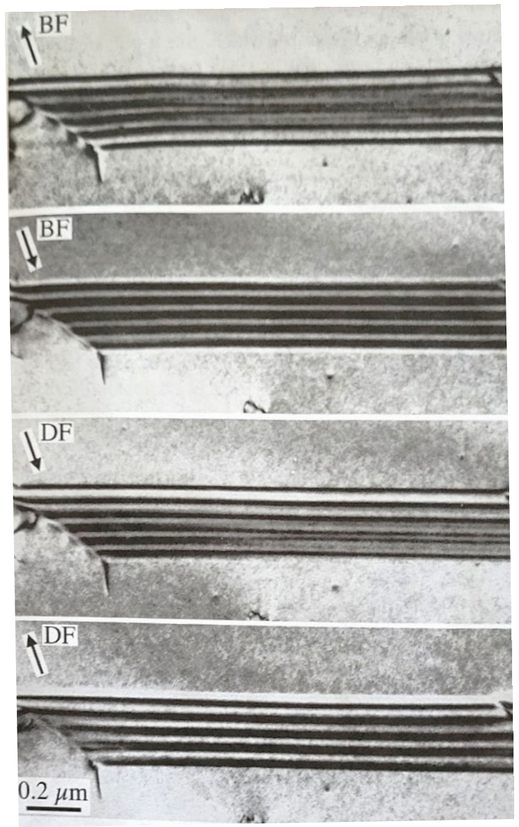

	$\boldsymbol{R(r)}$	$\boldsymbol{g}$	$\boldsymbol{2\pi g \cdot R}$
SF in FCC	$1/3[111]$	(111), (220),(113)	$2\pi/3$
SF in FCC	$1/6[11\bar{2}]$	(111) (220)	0 $4\pi/3$

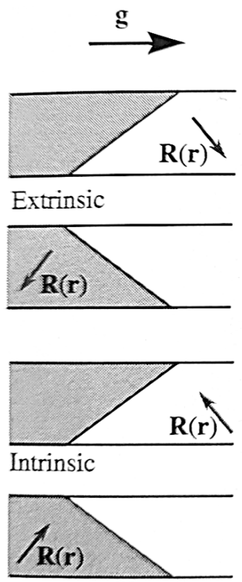

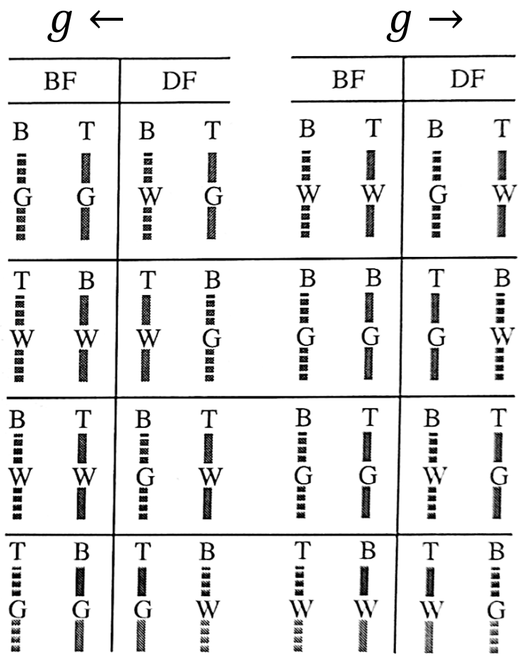

$$\frac{d\phi_g}{dz} = \frac{\pi i}{\xi_g}\phi_o(z)' + 2\pi i s_R \phi_g(z)' \text{ and}$$

$$s_R = s + \boldsymbol{g} \cdot \frac{\boldsymbol{dR(r)}}{dz}$$

Scanning (S)TEM imaging of defects

Focused e^- probe scanned on sample; disc and annular detectors in back focal (diffraction) plane

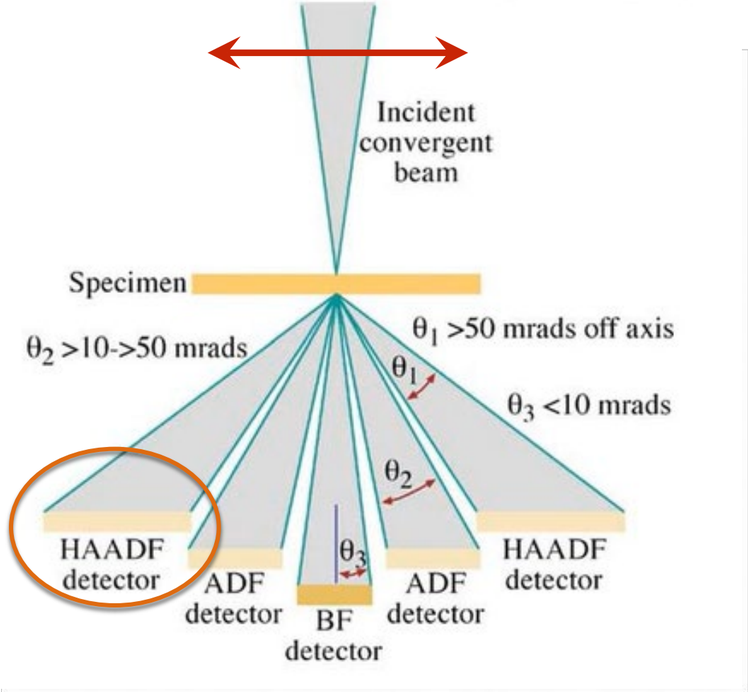

High-angle annular dark-field => compositional contrast:
intensity $\propto Z^2 t$
(thickness t, atomic number Z)

Z-contrast examples:

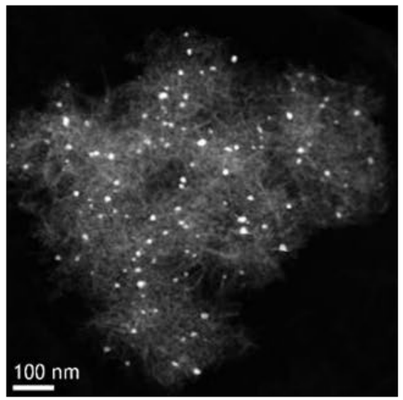

Pt catalyst on Al_2O_3

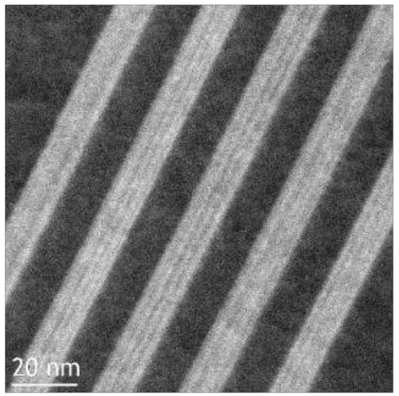

Si-Ge/Si multilayer

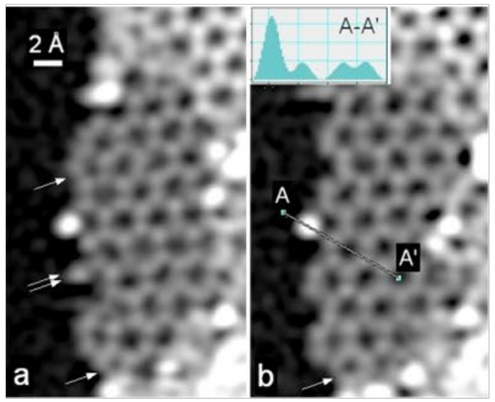

Cs-orcrected - graphene with dopant atoms (Krivanek et al., Nion)

STEM imaging mode suppresses bend contours

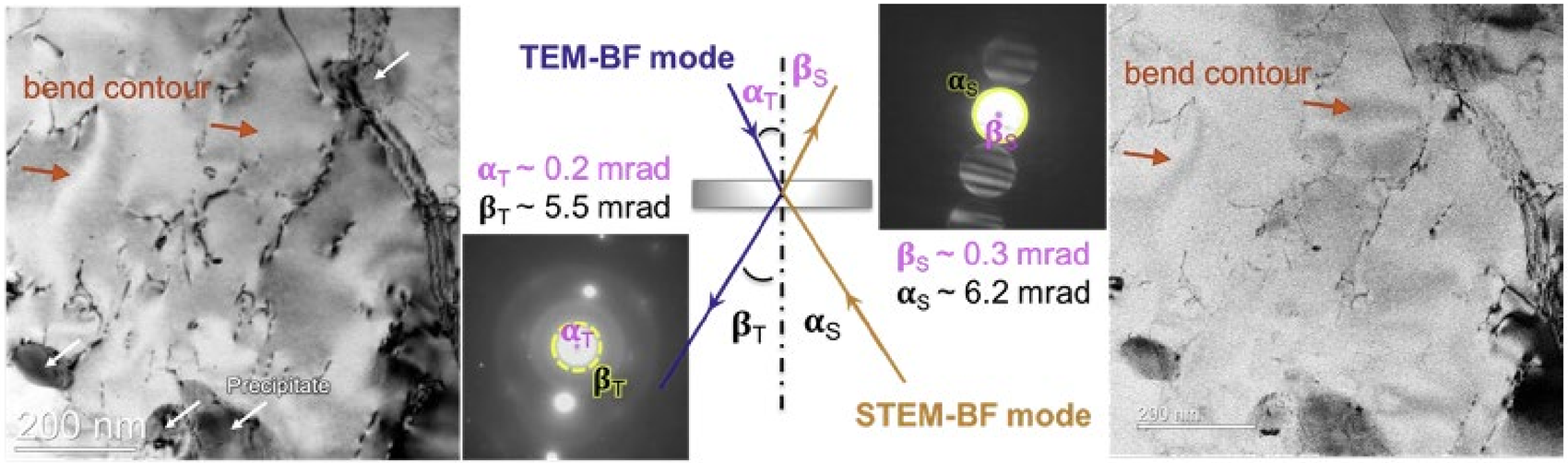

Bend Contour contrast is suppressed when $\beta_S \approx \alpha_S$

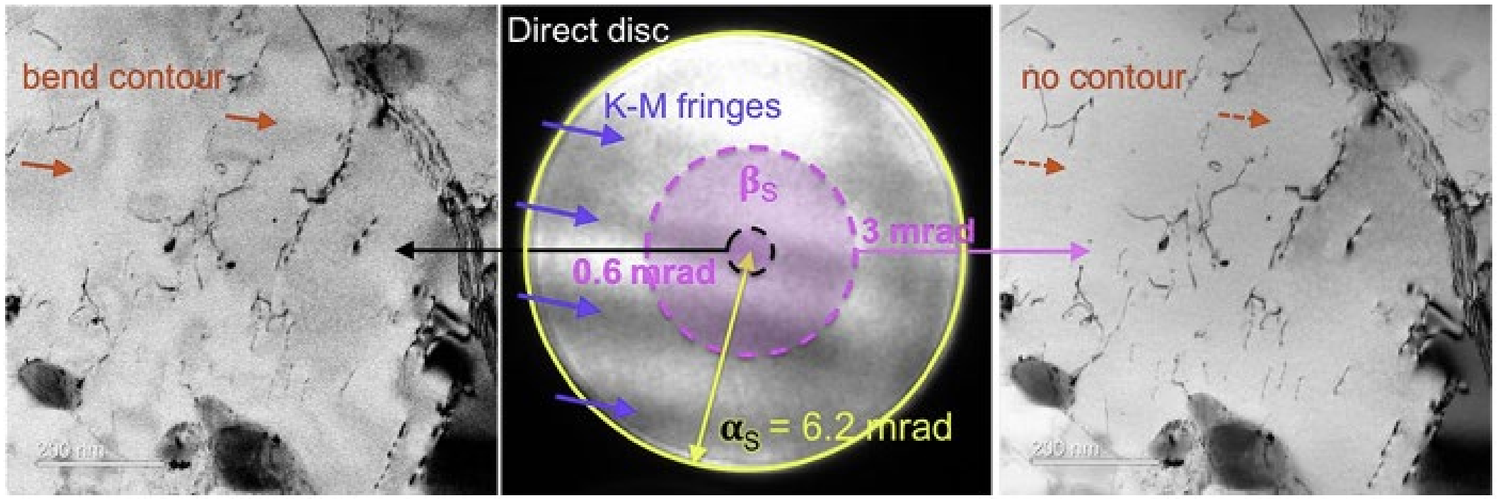

Dislocation Density Measurements

HAADF $\beta_S(24mrad) \approx \alpha_S(20\text{mrad})$

$\Lambda \approx 5\text{X}10^9\ \text{cm}^{-2}$

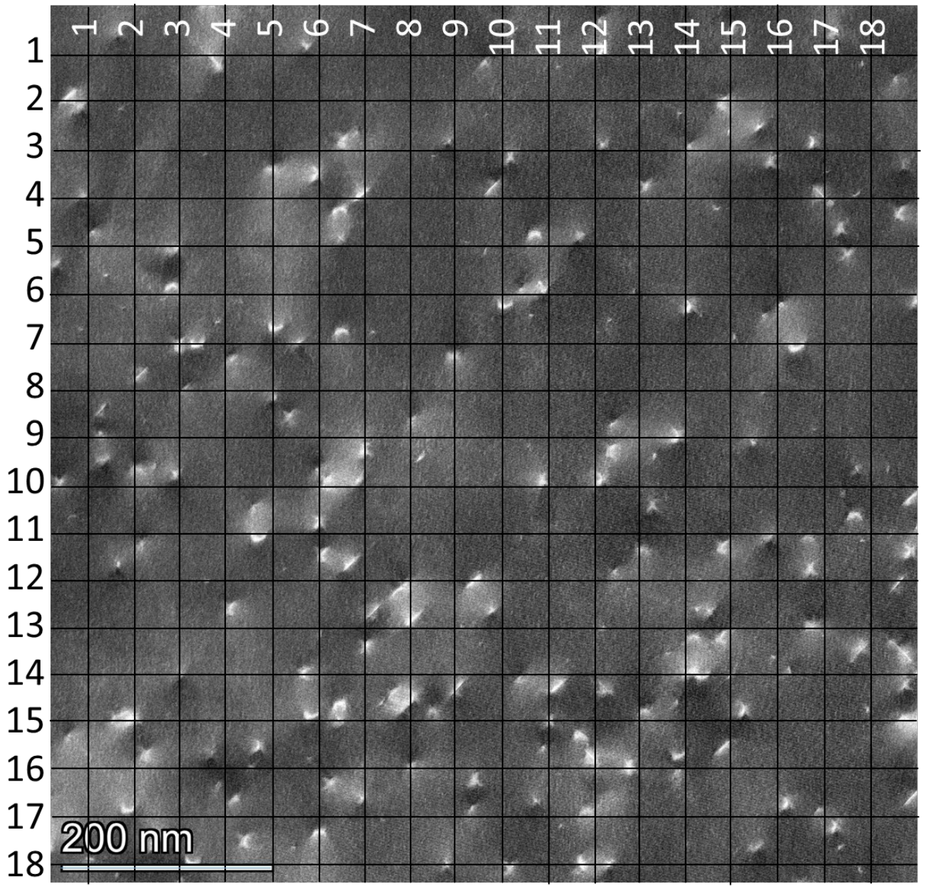

Line Intercept Method

- Make a grid having a total line length L
- Count the number of intersections between a given grid and the dislocations, N
- Measure TEM sample thickness, t (EELS, CBED, X-ray reflectivity, etc.)
- The dislocation density, Λ, is given by the following equation.

$$\Lambda = 2N/tL$$

- This method is valid for dislocation density is less than $10^{14}\ \text{cm}^{-2}$.

HR-STEM images of stacking faults

Growth faults in AlN nanowires

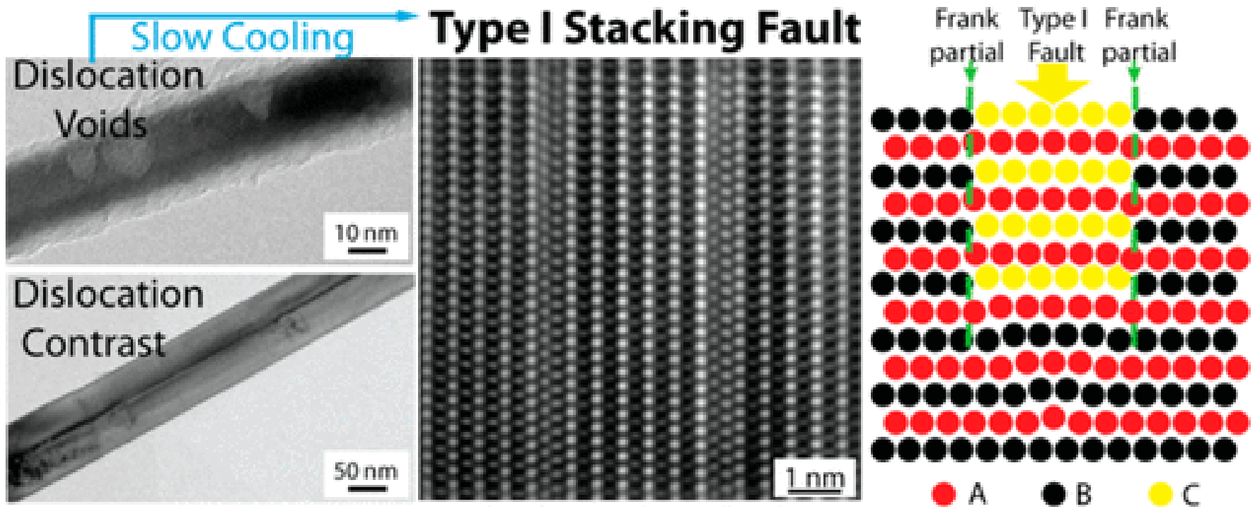

Stacking Fault Tetrahedron in FCC Superalloy

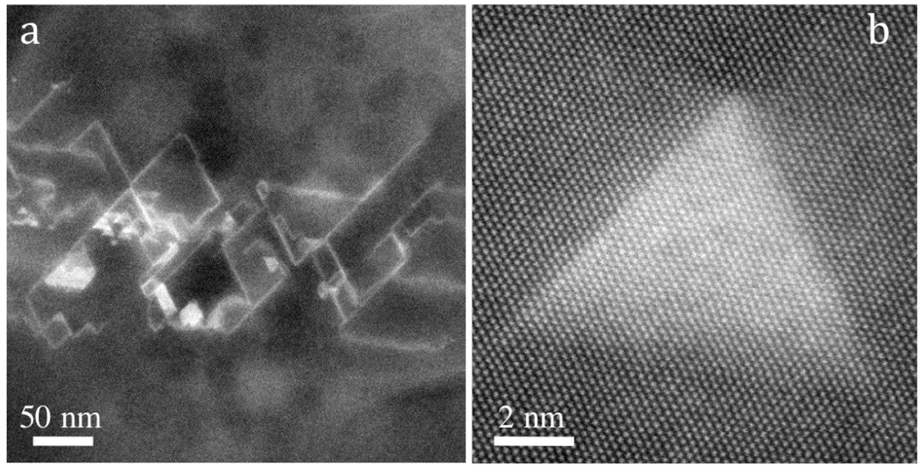

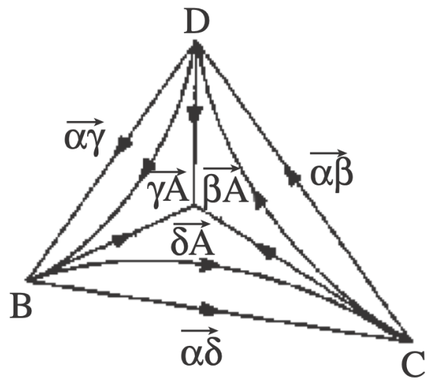

HR-STEM images of the Dislocations

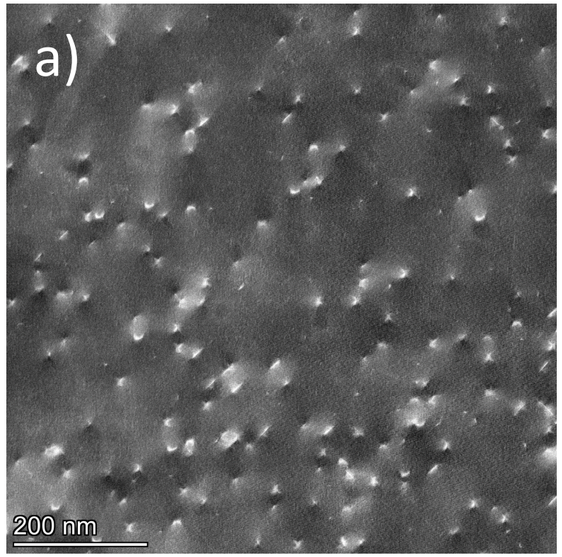

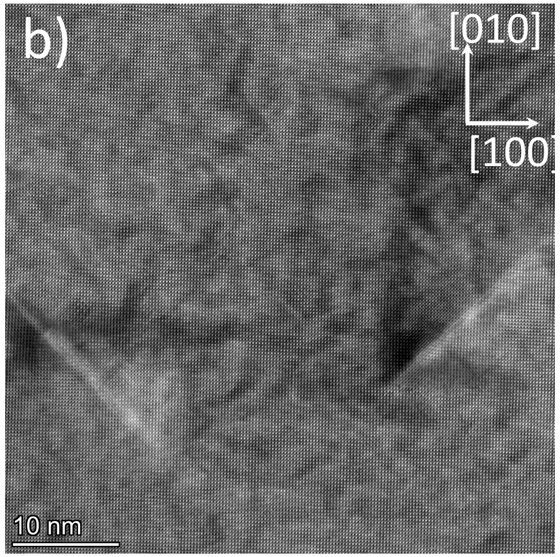

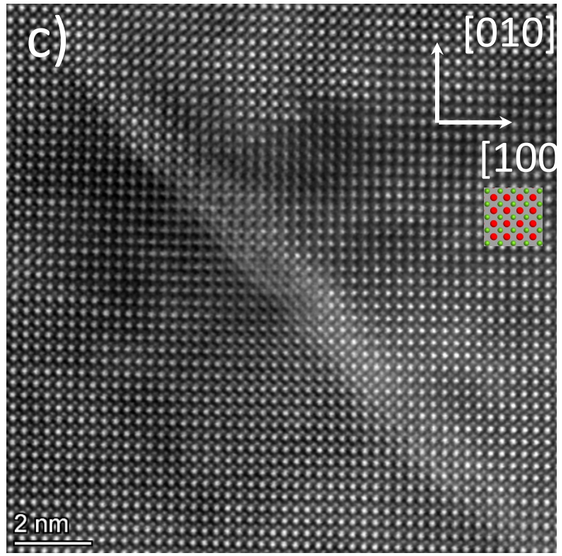

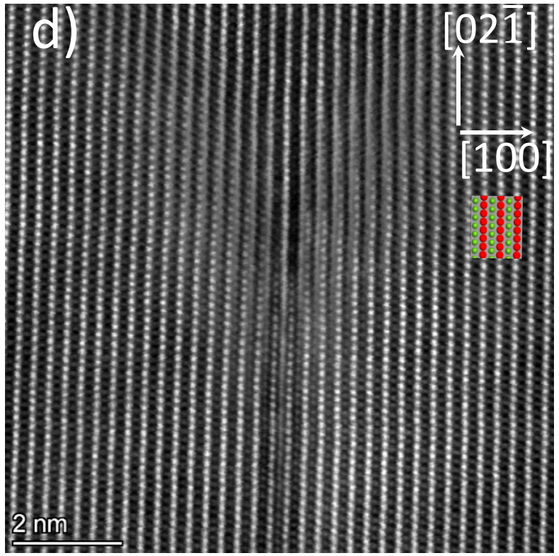

Fourier Filtering

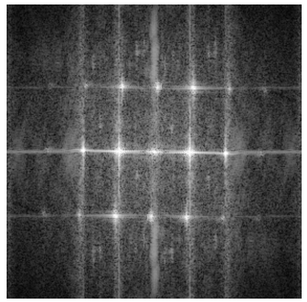

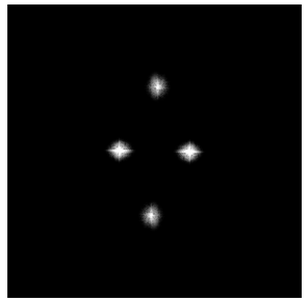

$\vec{b} = a[100]$

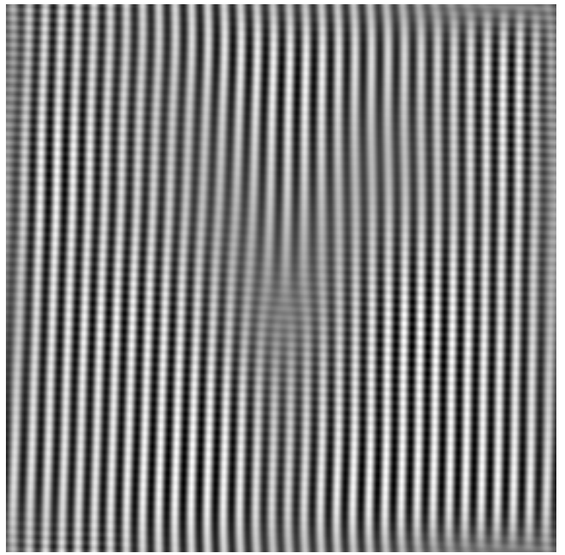

$\vec{b} = a[111]$

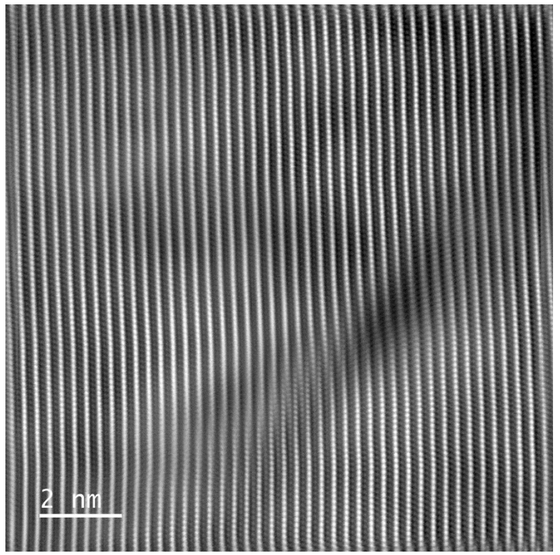

Geometric Phase Analysis of Dislocations

HR-TEM image

FFT filtered image

Phase image

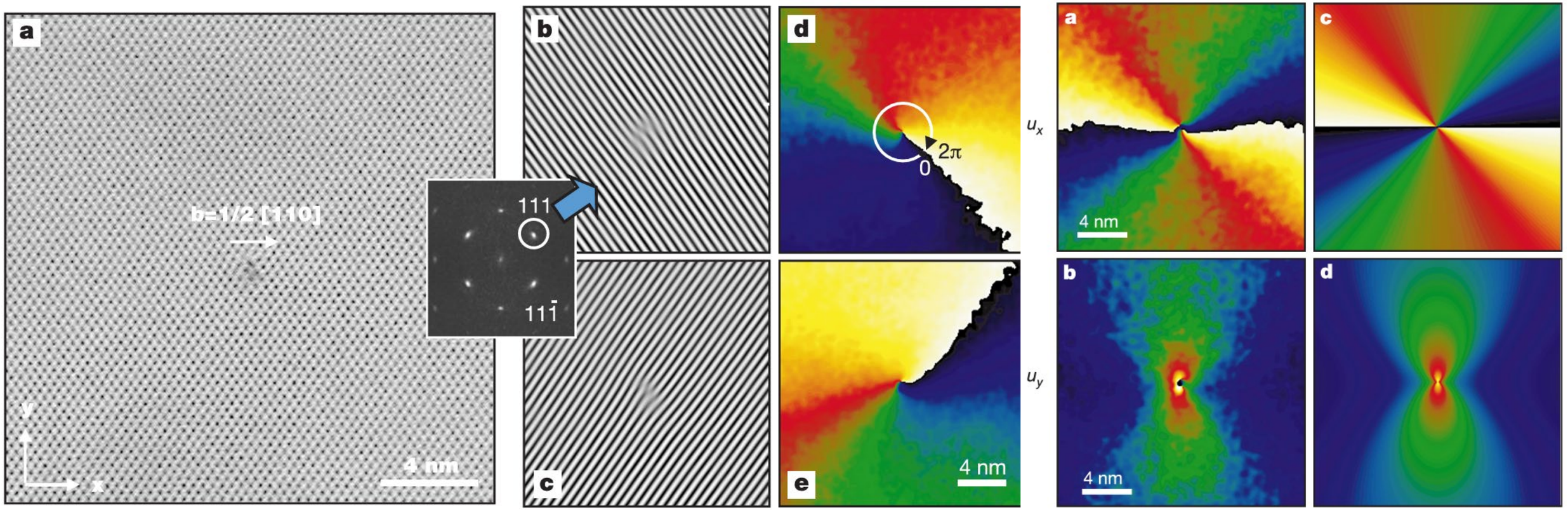

$$u_x = \frac{b}{2\pi}\left(\theta + \frac{\sin 2\theta}{4(1-\nu)}\right) \qquad u_y = -\frac{b}{2\pi}\left(\frac{1-2\nu}{2(1-\nu)}\ln r + \frac{\cos 2\theta}{4(1-\nu)}\right)$$

HR-STEM images of the Dislocations

Table 1
Observed slip system in the eight B2 alloys studied.

Alloy	CuZn	FeAl	NiAl	FeTi	CoTi	NiTi	FeGa
Dominant slip directions	⟨1 1 1⟩	⟨1 1 1⟩	⟨0 0 1⟩ ⟨1 1 1⟩	⟨0 0 1⟩	⟨0 0 1⟩	⟨0 0 1⟩	⟨1 1 1⟩
References	[1–5]	[6–11]	[5,12–16]	[17]	[18–23]	[9,24–27]	[28]

Table 2
Calculated and experimental lattice parameters a (Å) and elastic moduli (GPa).

Alloy	CuZn	FeAl	NiAl	FeTi	CoTi	NiTi	FeGa	PdAl
a (this work)	2.97	2.88	2.90	2.95	2.97	3.01	2.90	3.02
a (experiment) [58]	2.95	2.91	2.88	2.98	2.99	3.01	2.91 [55]	3.04
C_{11} (this work)	123.3	254.4	204.1	384.8	212.6	185.3	240.4	221.8
C_{11} (experiment)	119	194	199	310	203	162	NA	NA
C_{12} (this work)	107.3	136.1	133.2	102.8	169.5	149.7	150.2	160.9
C_{12} (experiment)	102	116	137	86	129	132	NA	NA
C_{44} (this work)	83.4	139.6	114.5	68.2	52.2	48.6	115.7	92.9
C_{44} (experiment)	74	133	116	75	68	71	~100	NA
References for experiments	[59]	[60]	[61]	[62]	[63]	[64]	[65]	

$$\vec{b} = a < 111 > \{110\} \quad \vec{b} = a < 100 > \{110\}$$

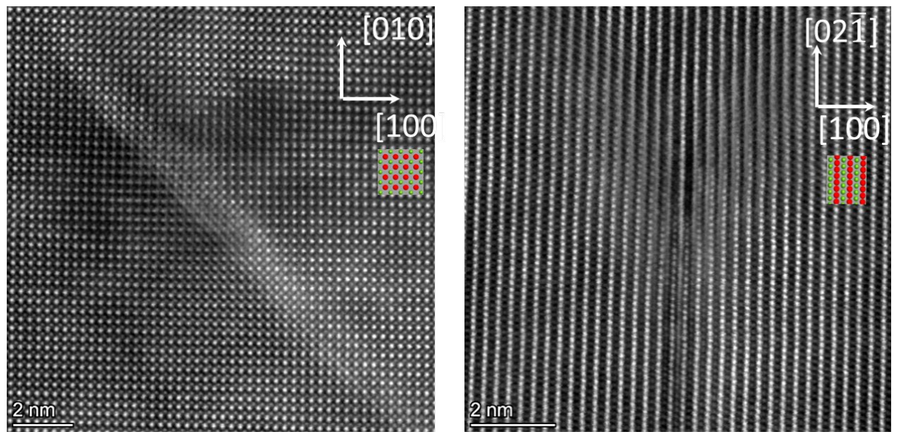

$$A = 2C_{44} \backslash (C_{11} - C_{12}) \qquad K^{screw} = \mu b^2 / 4\pi$$

$$W \approx \frac{\mu b^2}{4\pi} \ln \frac{R}{r_0} \to \infty \quad r_0 \to 0$$

Table 3
Anisotropy factors A and energy factors K (J/m $\times 10^{-9}$) determining the elastic energy of corresponding dislocations per unit length (m).

Alloy	A	$K^{screw}_{\langle 111\rangle}$	$K^{edge}_{\langle 111\rangle}$	$K^{screw}_{\langle 001\rangle}$	$K^{edge}_{\langle 001\rangle}$	$K^{screw}_{\langle 111\rangle}/K^{screw}_{\langle 001\rangle}$
CuZn	10.42	0.369	1.130	0.585	0.405	0.63
FeAl	2.36	1.531	2.766	0.921	0.855	1.66
NiAl	3.23	1.028	2.152	0.766	0.671	1.34
FeTi	0.48	2.252	2.611	0.473	0.939	4.76
CoTi	2.42	0.606	1.328	0.366	0.438	1.66
NiTi	2.73	0.535	1.212	0.350	0.402	1.53
FeGa	2.56	1.218	2.388	0.774	0.750	1.57
PdAl	3.05	0.946	2.066	0.674	0.664	1.40